DNA 2737
ATR-71-25

LOFTING OF PARTICULATES BY A HIGH SPEED WIND (U)

by
BRUCE HARTENBAUM

SEPTEMBER 1971

PREPARED FOR

DEFENSE NUCLEAR AGENCY
WASHINGTON, D.C. 20305

UNDER CONTRACT DASA01-70-C-0041

1010 WESTWOOD BOULEVARD
LOS ANGELES, CALIFORNIA 90024
Telephone (213) 479-4379

Applied Theory, Inc.

Unclassified

Security Classification

DOCUMENT CONTROL DATA - R & D

(Security classification of title, body of abstract and indexing annotation must be entered when the overall report is classified)

1. ORIGINATING ACTIVITY (Corporate author) APPLIED THEORY, INC. 1010 Westwood Boulevard Los Angeles, California 90024	2a. REPORT SECURITY CLASSIFICATION Unclassified 2b. GROUP N/A

3. REPORT TITLE

LOFTING OF PARTICULATES BY A HIGH SPEED WIND

4. DESCRIPTIVE NOTES (Type of report and inclusive dates)

Final Report

5. AUTHOR(S) (First name, middle initial, last name)

Bruce Hartenbaum

6. REPORT DATE	7a. TOTAL NO. OF PAGES	7b. NO. OF REFS
September 1971	73	22

8a. CONTRACT OR GRANT NO.	9a. ORIGINATOR'S REPORT NUMBER(S)
DASA01-70-C-0041 b. PROJECT NO. NWER XAXS c. Task and Subtask: A001 d. Work Unit: 02	ATR-71-25 9b. OTHER REPORT NO(S) (Any other numbers that may be assigned this report) DNA 2737

10. DISTRIBUTION STATEMENT

Approved for public release;
distribution unlimited.

11. SUPPLEMENTARY NOTES	12. SPONSORING MILITARY ACTIVITY
	Director, Defense Nuclear Agency Washington, D.C. 2035

13. ABSTRACT

Wind tunnel studies of particulate lofting were conducted at free stream speeds of between 112 and 376 fps. Measurements were made of the rate at which particulates were lofted, of the wind velocity profile and of the number density of airborne particulates. The measurement bearing the most practical significance was that of the lofting rate; the measured lofting rate was only 1/10 that of the maximum rate predicted by current theory, although the lofting rate was found to be directly proportional to the shear stress velocity in accord with the theory. The velocity profile within the boundary layer but at heights greater than the effective roughness created by the particulate flow is of the form given by Prandtl's law for flow past a wall. Boundary layer calculations in conjunction with the measurements show that Owen's form for the flow law cannot hold near the head of the boundary layer.

DD FORM 1 NOV 68 1473 REPLACES DD FORM 1473, 1 JAN 64, WHICH IS OBSOLETE FOR ARMY USE.

Unclassified

Security Classification

14. KEY WORDS	LINK A		LINK B		LINK C	
	ROLE	WT	ROLE	WT	ROLE	WT
Dust Pickup Particulate Lofting Solif-Gas Flows						

DNA 2737
ATR-71-25

LOFTING OF PARTICULATES BY A HIGH SPEED WIND (U)

This effort supported by Defense Nuclear Agency
Under NWER, Subtask Code SA001, Work Unit Code 02

by

Bruce Hartenbaum

PREPARED FOR

DEFENSE NUCLEAR AGENCY
WASHINGTON, D.C. 20305
Under Contract DASA01-70-C-0041

September 1971

APPLIED THEORY, INC.
1010 Westwood Boulevard
Los Angeles, California 90024

ABSTRACT

Wind tunnel studies of particulate lofting were conducted at free stream speeds of between 112 and 376 fps. Measurements were made of the rate at which particulates were lofted, of the wind velocity profile and of the number density of airborne particulates. The measurement bearing the most practical significance was that of the lofting rate; the measured lofting rate was only 1/10 that of the maximum rate predicted by current theory, although the lofting rate was found to be directly proportional to the shear stress velocity in accord with the theory. The velocity profile within the boundary layer but at heights greater than the effective roughness created by the particulate flow is of the form given by Prandtl's law for flow past a wall. Boundary layer calculations in conjunction with the measurements show that Owen's form for the flow law cannot hold near the leading edge of the boundary layer.

FOREWORD

The research program reported here was sponsored by the Defense Atomic Support Agency (DASA) under Contract DASA01-70-C-0041 and was performed during the period May 1970 to June 1971. The DASA contracting officer's representative was Mr. Clifford B. McFarland.

The Principal Investigator for the program was B. Hartenbaum. Others who contributed to the research were W. Gordy who built the apparatus, L. Walitt, M. Chapman and L. Glenn who aided in the aerodynamic design of the experiments and the staff of the Fluid Dynamics Laboratory of the Lockheed-California Company Rye Canyon Research Laboratory where the experiments were performed.

NOMENCLATURE

A	area
A^*	area at sonic flow
c_f	local friction coefficient
d	diameter
g	acceleration of gravity
M	mass of particulates per unit area
$\dot{M}$	mass lofting rate lbm/(ft^2-sec)
a	reciprocal of exponent in power law velocity profile
v_p	vertical velocity of particulate
u_o	free stream velocity
u_*	shear stress velocity
x	axial coordinate
y	vertical coordinate
δ	boundary layer thickness
δ^*	displacement thickness
θ	momentum thickness
ρ_g	gas density
τ	time constant
d	diameter of particulate
I	light intensity - watts/steradian
I_o	initial light intensity - watts/steradian
K_x	total scattering coefficient (total scattering cross section ÷ geometric cross section)
ℓ	path length
n	number density - number/cm^3
r	radius of particulate
α	$\lambda/2\pi r$
λ	wavelength
φ	angle
φ_d	angular radius of Airy's disc

TABLE OF CONTENTS

LIST OF ILLUSTRATIONS

LIST OF ILLUSTRATIONS (Continued)

LIST OF ILLUSTRATIONS (Continued)

SECTION 1

INTRODUCTION AND SUMMARY

In the past, attempts have been made to calculate the mass and velocity of a) debris thrown out directly from the crater resulting from a nuclear explosion and b) the debris lofted outside the crater by the high speed wind produced by the same nuclear explosion. The latter problem is the concern of this research. The lofting calculations were based in part upon meteorological and laboratory data obtained with low speed winds which were extrapolated to the very high wind speeds characteristic of nuclear explosion phenomena, and in part upon a theoretical model of the lofting process. The purpose of this program was to obtain for the steady state lofting process high speed laboratory data which could be used to increase the accuracy of the theoretical model. The nuclear problem is very complicated; the problem addressed here was highly idealized in an attempt to uncover and understand the basic aerodynamics of the lofting process. To this end the experiments were performed in a wind tunnel with the ground surface idealized by a bed of finely graded, noncohesive silica particles. For the tests to have meaning in the context of lofting on a meteorological scale the wind tunnel was made large enough so that the boundary layer did not occupy an appreciable fraction of the tunnel height and so that the number of particulates striking the roof of the tunnel was so small that their presence did not perturb the flow.

Three tests were performed at free stream speeds of 111.8, 237.8 and 371.3 fps which placed the particulate motion in the

suspension regime (the ratio of the drag force based on the shear stress velocity to the weight of the particulate was 3.3, 17.4, and 88.0 at the three wind speeds). Measurements were made of the rate at which particulates were lofted, of the velocity profile, and of the number density of lofted particulates. The measurement bearing the most practical significance was that of the lofting rate; the measured lofting rate was only 1/10 the maximum rate predicted by the theoretical model. The lofting rate was found to be directly proportional to the shear stress velocity, in accord with the model. The difference between the calculated and the measured lofting rate does not imply that the model is invalid, but rather that the experiments can be used within the framework of the model to set the efficiency of conversion of the horizontal impulse delivered to the ground surface by the wind to the vertical momentum of particulates. The calculation, aimed at maximizing the lofting rate, set this conversion efficiency at 100%; the experiments imply that the conversion process is only 10% efficient. Whether or not all of the details of the model are correct requires more extensive experimentation. The design phase of the present work, however did point out a deficiency in the calculation presented in Reference 8; namely, Owen's relation, Eq. 4, was applied without regard to the actual height of the boundary layer. The calculation of gas motion, which was inviscid, did not account for the growth of the boundary layer behind the initial blast wave and the subsequent velocity profile arising from the afterwinds.

The measured velocity profiles were interpreted in accord with the law for flow past a wall, with Owen's[1] relation providing a bridge between the test at 111.8 fps and the low speed tests performed in the saltation regime by other investigators. Owen's relation did not hold for the two higher speed tests; boundary layer theory indicated that Owen's law cannot apply near the leading edge of the boundary layer.

SECTION 2

EXPERIMENTAL TECHNIQUES

2.1 TEST SETUP

Steady state lofting tests were performed inside a rectangular cross section wind tunnel with a 40" height, 18" width and 26'8" length (Figure 1). A 4'-long circular-to-rectangular transition section joined the tunnel to Lockheed-California Company's 48" cross wind nozzle. A particulate bed approximately 4" deep at the start of each test was composed of AFS 50-70 Ottawa silica testing sand (mean particulate diameter: .25 mm). Design details of the steady state tunnel along with that of a transient tunnel are given in Appendix I. Lofting measurements were made within a diagnostics section which extended between 16' and 18'6" from the leading edge of the particulate bed. The location of the diagnostics section was determined as a compromise between placing the measurements station at least 10 hydraulic diameters downstream of the entrance and fitting the tunnel into the available space. The velocity profile of the wind was obtained from differential pressure measurements utilizing a rake containing 8 coaxial pitot tubes and 3 static tubes. The density profile of the lofted particulates was inferred from light extinction measurements. The position of the eroding ground surface needed for the velocity and density measurements was obtained photographically using a Locam camera. The lofting rate was obtained from measurements of the change in the level of the particulate bed during a test and the test time (Appendix II). Pressure, light intensity and gas temperature measurements were recorded using Lockheed-California Company's central data system. Each channel employed a 10 cps low pass filter and was sampled at a rate of 40/sec.

2.2 DIAGNOSTICS

2.2.1 Particulate Number Density

Under certain conditions, which are described below, the density of particulates contained within a beam of radiation can be ascertained by application of the Bouguer-Beer relation,

$$I = I_o \exp(-n\pi r^2 K_x \ell) \qquad (1)$$

to the results of light transmission experiments. To do so requires, first of all, that the Bouguer-Beer relation hold for the experimental setup. The main effort in this phase of the research was to design the extinction experiment such that Eq. 1 could be applied in a meaningful way to the results of the experiment.

It is clear from the derivation of Eq. 1 that in each differential element of length dx a quantity of light equal to $In\pi r^2 K_x dx$ is scattered out of the beam, but that no radiation is scattered into the beam; hence, strict application of this relation requires that the particulates be sufficiently diffuse or that the path length be sufficiently short that multiple scattering effects be negligible. A light transmitter and receiver were built with a light path of variable length in order to detect multiple scattering effects. It is assumed that if multiple scattering is involved in the scattering process when the beam length is equal, say, to the full width of the tunnel, then there exists some shorter distance for which only single scattering is involved. Secondly, the total scattering coefficient, K_x, must be known. In general, K_x depends on both

the ratio (denoted by α) of the particle circumference to the wavelength of the radiation, and on the refractive index of the particle relative to that of the surrounding medium. The refractive index will be a real quantity for a lossless material, but will be complex for a lossy (absorbing) material. For a lossless material, K_x is an oscillatory function of α which approaches the value 2 for $\alpha \gg 1$, while for a lossy material, K_x is heavily damped but still approaches $K_x = 2$ for large α. For the experiments at hand, typically $r = 125\mu$ and taking $\lambda = 550$ nm (green light) as an average value yields $\alpha = 1430$. For this large value of α, $K_x \simeq 2$ independent of α and the refractive index. That K_x approaches 2 rather than 1 can be seen more readily by application of geometrical and physical optics to the scattering process, than by applying the rigorous Mie theory for $\alpha \gg 1$. For transparent spherical particles the scattered light is composed of reflected, refracted, and diffracted light. The reflected and refracted components result from light incident on the projected area of the particle and would yield $K_x = 1$ if these were the only components of the scattered light. However, by Babinet's principle an amount of light equal to that incident on an opaque disc with area equal to that of the projected area of an opaque particle is diffracted around the particle. Thus, $K_x = 2$. Exact Mie scattering calculations have shown that diffraction theory for an opaque circular disc is a very good approximation for diffraction by a transparent particle.[2] Approximately 82% of the diffracted light falls within Airy's disc. A good rule of thumb, then, for practical design is that the diffracted light falls within Airy's disc. A more exact

relation based on Rayleigh's[3] result for the fraction of light falling outside a cone of half angle φ gives an apparent total scattering coefficient of $1 + [J_o(\alpha\varphi)]^2 + [J_1(\alpha\varphi)]^2$ for φ small ($\sin\varphi \sim \varphi$), where J_o and J_1 are Bessel functions of the first kind, of order zero and one, respectively. The angular radius of Airy's disc, given by $\varphi_d = 1.22\ \lambda/d$, is 0.152 degrees for a 250μ particle illuminated with green light (λ = 550 nm). Unless the angular aperture of the light detector is considerably smaller than φ_d the apparent total scattering coefficient will be less than 2. The approach adopted here is to make the angular aperture of the receiver optics several times that of φ_d to ensure that all of the diffracted light is collected. The angular aperture must not be so large, however, as to collect a significant amount of the refracted and reflected light. For a spherical particle geometric optics implies that the ratio of the intensities of refracted and incident light varies with angle according to the formula[4]

$$\frac{I_1}{I_o} = \frac{(1 - k_1)^2}{2} \frac{\sin 2i_1}{\sin\varphi} \frac{di_1}{d\varphi} \qquad (2)$$

where $\varphi = 2(i_1 - r_1)$

$$k_1 = \frac{1}{2}\left[\frac{\sin^2(i_1 - r_1)}{\sin^2(i_1 + r_1)} + \frac{\tan^2(i_1 - r_1)}{\tan^2(i_1 + r_1)}\right]$$

$$\frac{di_1}{d\varphi} = \frac{\sin i_1 \cos r_1}{2 \sin\left(\frac{\varphi}{2}\right)} \ ;$$

r_1 is the angle of refraction and i_1 is the angle of incidence. The angular variation of the reflected light is

$$\frac{I_2}{I_o} = \tfrac{1}{2} k_2 \qquad (3)$$

where $$k_2 = \frac{1}{2}\left[\frac{\sin^2(i_2 - r_2)}{\sin^2(i_2 + r_2)} + \frac{\tan^2(i_2 - r_2)}{\tan^2(i_2 + r_2)}\right]$$

$$\varphi = \pi - 2i_2;$$

r_2 is the angle of reflection corresponding to i_2.

The dependence on angle of the ratio of the sum of the refracted and reflected intensities to the incident intensity (Figure 2), indicates that the measurement error will be small provided that the angular aperture is less than 1 degree. It has already been shown that an angle of 0.152 degrees is sufficient to collect the diffracted light.

In addition to providing a proper value for the angular aperture, all particles must see the same angular aperture. In other words, the entrance pupil of the light receiver must be large enough so that light scattered within an angle equal to the acceptance angle of the receiver will be detected even if the light comes from a particle at the outermost edge of the beam and at the axial location farthest from the receiver.

A system employing these design criteria is illustrated in Figure 3.

The diameter of the transmitter tube was selected as a compromise between having a large diameter beam to sample many particles and a small diameter probe to minimize flow disturbances

when inserting the probe into the flow. The receiver tube diameter is fixed by the beam diameter and the required entrance pupil diameter. The angular aperture of the receiver is 0.375 degrees while the theoretical beam spread is 0.24 degrees.

As noted above the problem of most concern to the proper interpretation of the light extinction data was that of multiple scattering. Prior to performing the full scale tests in the 40" x 18" tunnel, tests were run in a 12" x 12" tunnel to ascertain if multiple scattering was important. The effects of multiple scattering were sought by comparing average densities measured with different path lengths. The measurements required that the probes be inserted into the flow. These small scale tests indicated that multiple scattering was not important for particulate densities of the order of $10/cm^3$ with a path length of 26 cm. The full-scale tests, performed at higher speeds than the small-scale tests, resulted in some cases in a much larger cutoff of light. Whether or not the Bouguer-Beer law holds under all full-scale test conditions remains to be established rigorously, although the fact that the full-scale test results are consistent among themselves (Section 3.3) implies that the Bouguer-Beer law does indeed apply. The light extinction apparatus was built to allow multiple scattering effects to be measured, but the limitation of the test program to three blows precluded making these measurements. Thus, during the full scale tests the length of the light beam was equal to the full width of the tunnel - 18 inches. Baseline shift during low speed runs was made very small by shielding the lenses from the dust-laden particulate flow, but at higher speeds simple passive shielding was less effective. At high speeds either an air flow directed outward from the front lenses or an electrostatic screen might prove helpful in reducing baseline shift.

2.2.2 Wind Velocity Profile

A rake containing eight pitot and three static tubes (Figures 4 and 5) was used to measure the velocity profile of the wind. The pitot tubes employed a coaxial design (Figure 6) to eliminate clogging of the tube by particulates. A fast time response was designed into the gauge by making the outer passageway large in area. By placing the pressure sensing element close to the front of the gauge, errors in the measured stagnation pressure arising from momentum exchange between the gas and particulates have been eliminated.[5] Particulates enter into, and are decelerated by, the inner tube without affecting the measured value of the stagnation pressure. A bleed hole at the end of the inner tube allows particulates to be removed from the inner tube; thus, the gauge test time is extended by increasing the time to fill the inner tube with particulates. The bleed hole area was made equal to 5% of the probe inlet area to minimize errors in the stagnation pressure measurement.[6] A pitot-static tube was not built although a triaxial tube can be readily conceived. The static pressure was obtained from three static tubes located at different positions along the rake which also held the eight pitot tubes. In addition to supplying a static reference pressure the three static tubes were used to determine whether or not streamline curvature in the boundary layer introduced a vertical pressure gradient into the flow.

The total and static pressures were measured with Statham PM 131TC differential pressure transducers with full scale ranges of either 2.5 or 5.0 or 7.5 psia. These gauges were adequate for the required task but required a careful calibration at low pressures employing a water manometer. The total differential

pressures measured during the tests ranged between 0.005 and 1.17 psid. The acoustic time constant of the pitot tube system was of the order of 7 msec, which was much faster than required and resulted from pre-test underestimates of the test time.

SECTION 3

RESULTS

3.1 VELOCITY PROFILE IN THE BOUNDARY LAYER

The velocity profiles for free stream velocities of 111.8, 237.8 and 376.3 fps are shown in Figures 9 to 11. The velocity within the boundary layer is fitted well by a power law (Figure 12), such that $u \alpha y^{1/a}$, with a = 1.61, 1.36, and 1.57 at u_o = 111.8, 237.8 and 376.3 fps respectively. A semi-log plot of the velocity profile (Figure 13) reveals, however, that the flow may be interpreted on the basis of the law for flow past a rough wall. The three sets of data intersect at y = 1.65 in., u = 30 fps. This intersection is qualitatively similar to the focus of Bagnold[9] and Zingg[10] but occurs at a greater height and larger velocity; the concept of a focus is therefore approximate at best. Moreover the constancy of wind speed below the so-called focus, found by Bagnold at low free stream wind speeds, was not observed at the high free stream wind speeds employed in these tests (Figure 13). The thickness of the velocity boundary layer at the pitot rake station, given in Figure 13 by the intersection of the two straight lines that characterize each velocity profile, varies between 9.5 and 15.2 inches as the free stream velocity varies between 111.8 and 376.3 fps.

The shear stress velocity, u_*, was inferred from the velocity profile assuming that the universal constant for turbulent flow past a wall, 5.75, properly described the experimental data. In other words u_* was determined by applying the relation $du/d(\log y) = 5.75u_*$. Thus the shear stress velocity was determined to be 16.3, 41.0 and 61.0 fps at a position 18 ft from the leading edge of the particulate layer at free stream speeds of 111.8, 237.8 and 376.3 fps

respectively. That the constant 5.75 is appropriate is also shown by plotting u/u_* vs log $y/(u_*^2/2g)$ (Figure 14). Data for the lowest speed run, 111.8 fps, falls on the straight line given by Owen[11] as

$$\frac{u}{u_*} = 5.75 \log_{10} \frac{y}{\frac{u_*^2}{2g}} + 9.7 \qquad (4)$$

However higher speed data do not satisfy Owen's relation. Eq. 2 predicts a minimum value of $u/u_* = 5$,[12] but in fact much of the data fall below this value. Boundary layer theory (Appendix I) makes it clear that Owen's relation cannot hold near the leading edge of the boundary layer.

3.2 RATE OF LOFTING OF PARTICULATES

The rate at which particulates are lofted by a high speed wind is given experimentally by $\dot{M} = 0.366*10^{-2}\ u_o^{5/4}$ lbm/(ft^2-sec) (Figure 7). The variation of the rate of mass lofting with free stream velocity is about the same for both the measured and computed results, which implies that the mass lofting rate is directly proportional to the shear stress velocity (Appendix I). The relation between $\dot{M}$ and u_* (Figure 8), indicates that this is indeed the case with a least squares fit yielding $\dot{M} = (0.860*10^{-3}\ u_* - 0.01)$ lbm/(ft^2-sec). The implication that no mass is lofted for shear stress velocities less than 1.16 fps is in qualitative agreement with threshold values determined by low speed tests.[7]

That the measured values of $d\dot{M}/du_o$ are the same as those computed with vertical particle velocity equal to u_* strongly suggests that the initial upward velocity of the particulates is proportional to u_* throughout the range of wind speeds tested. That the experimentally determined rate of lofting is an order of magnitude less than the computed rate implies that the conversion of horizontal

impulse at the ground surface to vertical momentum of particulates is rather inefficient. It should be borne in mind that the parameter used in the lofting model to relate the initial velocity of the particulate to the shear stress velocity was extrapolated from low speed tests and that the parameter used to relate shear stress to upward momentum was chosen to maximize the lofting rate. At present, it appears that the correct value of the latter parameter is about 1/10 of the assumed value.[8]

3.3 DENSITY OF LOFTED PARTICULATES

The density of lofted particulates was inferred from light extinction measurements (Figures 15 to 17), using single scattering theory (Section 2.2.1). The density profiles at wind speeds of 111.8, 237.8 and 371.3 fps shown in Figure 18 correspond to the times at which the velocity profiles (Figures 9 to 11) were measured. A linear baseline shift correction was made to the data in the calculation of the densities, but the rate of shift of the baseline with time was not measured; it is noted that the error in the derived density introduced by the shift is made less severe by the logarithmic relation between transmittance and particulate density. The error does not exceed 25 percent.

As a rough check on the accuracy of the density measurements and on the overall consistency of all of the measurements the mass flux of particulates across the cross-section of the tunnel was calculated and compared with the rate of removal of mass upstream of the diagnostics station at a wind speed of 112 fps. The flux was calculated from the measured densities of lofted particulates (and straight line extrapolations to $y = 0$, $n = 100/cm^3$ and $y = 19.6''$, $n = 0$) and by assuming that at any given height the particulates were transported downstream at the

local gas velocity (a straight line extrapolation of the log-log velocity plot was used at small values of y). The flux calculated in this manner was less than, but within 15% of the lofting rate calculated from the rate of depletion of the particulate bed.

SECTION 4

CONCLUSIONS AND RECOMMENDATIONS

The conclusion of greatest practical significance is that the amount of wind-lofted debris is only 1/10 the maximum value predicted by the present crude theory. That aspect of the model which directly relates the rate of lofting of the mass to the shear stress velocity is borne out by the experiments. The gas flow in the suspension regime is qualitatively similar to that found in the saltation regime by other investigators; namely, the velocity profile is represented well by the law for flow past a rough wall. However, Owen's form of the flow law was found experimentally to hold only under certain conditions. In addition, the design phase of this program made it appear that Owen's relation could not hold near the leading edge of the boundary layer. These two facts point out that a correct calculation of particulate lofting must account properly for the growth of the boundary layer. It is recommended that any future study of lofting include an analysis of the two-phase boundary layer growth with particulate lofting. Both the skin friction coefficient and details of the particulate motion must be determined to characterize adequately the properties of the boundary layer. The photographic determination of the trajectories of individual particulates is made difficult by the large concentration of particulates near the ground surface although a large scale vortical motion of the particulates is revealed by high speed photographs; a narrow strip of particulates may make photographic analysis of individual particulates possible. If so, then the relationship between flows in channels of different widths must also be understood. A high frequency particulate counter may prove useful for the determination of both number flux and particulate velocity.

Transient tests similar to those outlined in Appendix I may reveal that the mass of material lofted behind the shock wave is greater than that lofted during steady flow, and such tests should accordingly be undertaken. Because the steady flow experiments have now been performed, at least in part, a dual purpose tunnel is no longer important and a simple shock tube would suffice.

Most non-ideal effects such as a compacted surface, moisture and vegetation would make the lofting rate less than that measured. Thermal effects, on the other hand, may tend to increase the lofting rate. The effects of thermally-induced shock curvature and thermal gradients should be investigated to complete the survey of lofting.

APPENDIX I

WIND TUNNEL DESIGN

I.1 PRELIMINARY DESIGN

In the initial design of the lofting facility both transient and steady state tunnels were evaluated. Important factors considered in the designs were the rate of lofting of particulates, the interaction between particulates and the walls of the tunnel, the thickness of the boundary layer compared to the height of the tunnel, the test time and flow stability. The transient design was of particular interest at the outset of the program for several reasons. For example, by proper operation of a blow-down tunnel the flow could be made to pass through a transient phase initiated by a blast wave, and then reach a period of quasi-steady flow limited only by the capacity of the blow-down tanks and the rate of depletion of the particulate bed. Thus, the blow-down tunnel would not only supply the same data obtainable with a conventional steady state tunnel, but would also furnish data on the blast wave phase. Moreover, several inviscid calculations showed that the blow-down operation would reach the steady flow in the shortest possible time; namely, steady inviscid flow would be achieved directly behind the blast wave. However, the inclusion of viscous effects into the design study made it appear that the flow would be unstable. In addition, studies of the two-phase boundary layer made it appear that within the scope of extant theory, a high speed tunnel had to be very large; the two-phase boundary layer was estimated to be much thicker than an air boundary layer at the same free stream velocity. Thus, although it was thought at first that transient tests would make it possible to investigate lofting at very high speeds with a minimal investment in tunnel facilities, the possibility of flow instability and the large tunnel size required for high speed tests caused the transient tunnel concept to be discarded in favor of more modest speeds in a steady state tunnel.

I.1.1 Rate of Removal of Particulate Mass

The scale of the hardware required to study particulate lofting at a given wind speed is governed both by the boundary layer thickness and the rate of removal of particulates from the test bed. Following the model formulated in Reference 8 an upper bound to the particulate mass lofted under steady state conditions was calculated at the outset of the program. To review briefly the lofting model, the vertical momentum of the particulates lofted from a loose bed was set equal to some fraction of the horizontal impulse delivered to the ground plane by the wind in a unit time. In addition, the vertical velocity of the particles was set equal to some fraction of a quantity u_*, known as the shear stress velocity. For the purposes of estimating wind tunnel lofting both fractions were set equal to unity. Under the two stated assumptions - and recalling that the shear stress exerted on the ground surface by a wind of density ρ_g is by definition equal to $\rho_g u_*^2$ - we find that

$$Mv_p = Mu_* = \rho_g u_*^2 \, \Delta t,$$

where v_p is the vertical component of particle velocity; thus

$$M = \rho_g u_* \, \Delta t \tag{5}$$

A proper evaluation of Eq. 5 requires that the relation between the shear stress velocity and the free stream velocity be known. By assuming that the logarithmic law of the wall holds (Eq. 4), the relation between u_o and u_* can be obtained, but only through its dependence on the boundary layer thickness. In fact from Eq. 4 one can deduce a relation between u^2/y and u/u_*, so that

if u is known at some altitude y within the boundary layer, then u_* is determined; in particular u_* is determined explicitly given the free stream velocity u_o at an altitude equal to the boundary layer thickness δ. The relation between u_o^2/δ and u_o/u_* (Figure 19, with $y = \delta$ and $u = u_o$) indicates that an upper bound on M may be obtained without resorting to boundary layer calculations by setting $u_o/u_* = 5$, which yields the largest value of u_* for a given value of u_o (Section 3.2). Equation (5) then yields mass lofting rates of 12.2 and 6.6 lbm/(ft^2-sec) at free stream velocities of 800 and 430 fps, respectively. If particles are not redeposited on the test bed then the rate of removal of mass from the test station will be equal to the rate of lofting; such a situation is encountered under flow conditions that characterize the suspension region (Section I) which were in fact the conditions achieved in the experiments. Thus, maximum rates of change of the height of the test bed for free stream wind speeds of 800 and 430 fps are 1.25 and 0.69 in./sec, respectively. A typical test bed, which might be 20 ft long x 1.5 ft wide would then experience mass lofting rates of 0.275 and 0.148 tons/sec at 800 and 430 fps, respectively. Such large rates of mass removal, if they did indeed occur, would render impractical steady state tests at high wind speeds with a duration of a second or more. Skipping ahead for a moment, the results of a more detailed calculation of the mass lofting rate utilizing boundary layer theory compare closely with the estimate based on u_o/u_*, but as shown by the experimental results both mass lofting rates are gross overestimates.

I.1.2 Transient Test

The large mass lofting rates obtained as discussed in Para. I.1.1 led to consideration of a transient test with a limited test time. In this type of test an initial blast wave is followed by a uniform flow. The use of a blast wave is advantageous not only because data would be obtained on the interaction of such a wave with a particulate bed, but also because the blast wave will lead to steady flow in the shortest possible time.

Two transient flow techniques were investigated theoretically using a one-dimensional variable-area computer code. The first scheme utilized a test section with an initial pressure less than atmospheric. The blast wave strength can be adjusted to raise the test section pressure to 1 atmosphere, thereby matching the pressure at the tunnel exit (the acoustic impedances would be slightly different, however, depending upon the degree of shock heating). The duration of the test is limited either by depletion of the sand bed, or by the mass flow characteristics of the air source. The results of a typical machine calculation (Figure 20) illustrate the idealized sequence of events for this test. The plenum chamber, initially at a pressure of 20.7 psia, was connected to the test section, initially at a pressure of 10.58 psia, through a 10° nozzle with $A/A^* = 6.25$. A diaphragm was located at the throat. Upon rupturing the diapgragm a weak shock wave moved into the test section raising its pressure to 13.52 psia (the particular combination of test section and plenum initial pressures did not result

in matched exit conditions). At the same time a rarefaction moved back into the reservoir, inducing the gas to flow into the test section. After 1 millisecond the nozzle became over-expanded causing a shock to stand in the nozzle. The idealized inviscid flow at a given station in the test section reaches steady flow conditions immediately after the shock passes that station.

The second scheme utilized a test section at an initial pressure of 1 atmosphere. The plenum chamber pressure was adjusted to achieve the desired overpressure and flow velocity in the test section. The duration of the test was limited by the length of duct downstream from the test section and by the gas sound speed. Three test cases were calculated to investigate the effects of nozzle area ratio on the flow. The nozzle area ratios were 3.3, 4.3, and 5.35. The pressures within the flow field, in each case, are plotted in Figure 21. Each case was designed to yield an overpressure of approximately 10 psia which simulates conditions at 9500 feet from a 1 MT blast. As in the previous case, a blast wave propagated through the test section with a stationary shock located in the nozzle. The main difference between the two cases lies in the strength of the blast wave. The results of six calculations, three for each scheme, are listed in Table I.1.

TABLE I.1

SUMMARY OF TRANSIENT TUNNEL CALCULATIONS

Velocity fps	Static Pressure psia	Plenum Pressure psia	Initial Pressure psia	A/A*
191	13.5	20.7	10.58	6.25
413	15.14	46.7	9.55	6.25
724	11.75	71.0	4.78	6.25
431	25.2	82	14.7	5.35
430	25.2	66	14.7	4.3
416	25.2	50	14.7	3.3

The one-dimensional model does not give a complete picture of the flow, but must be supplemented by a knowledge of two-dimensional effects. In particular, the ideal discontinuity standing in the nozzle may not always occur. The pressure rise predicted by one-dimensional theory to occur across a discontinuity may in reality occur across a rather large distance enclosing oblique shocks and regions of mixed subsonic and supersonic flow. This extended region is often referred to as a pseudo-shock.[13] The pressure rise across the oblique shock system often encourages the fluid to leave the walls of the nozzle with resulting flow separation. Separation in steady state rocket nozzles has been treated in the literature[14-18]. The maximum theoretical pressure ratio that can be taken across a normal shock without separation is approximately 1.67 for a flow with $\gamma = 1.4$.[19] The shock-boundary layer interaction may be minimized and separation prevented by removing the boundary layer, but with a concomitant

increase in experimental complexity. To continue, however, even should separation occur in the nozzle it is almost certain that the subsonic flow will reattach downstream of the nozzle. In fact, certain test facilities employ a choked venturi or orifice plate to meter flow, relying on reattachment downstream to smooth out the flow.[20]

The important point here is that the test section must not be too close to the nozzle. Exactly what "too close" means is not quantitatively known at the present, but is probably of the order of 10 to 20 diameters. In addition, a limited amount of experimental data has been obtained[21] which shows a normal shock standing for approximately 50 millisec in a highly overexpanded nozzle (Figure 22). These data were taken using a hot shot tunnel employing a hydrogen-oxygen-nitrogen driver and a nozzle with $A/A^* = 1000$. The chamber conditions yielded a stagnation pressure of approximately 300 psia and a stagnation temperature of approximately $6000^{\circ}R$. The downstream section was evacuated initially. Although the test conditions are quite different from those needed for the lofting test these data suggest that a standing shock may occur for a limited period of time.

In summary, these findings indicate that during a transient test a normal shock may stand in the nozzle under some flow conditions. In a steady state test the flow will almost surely separate if the pressure rise across the shock is greater than about 1.67 – but even should separation occur, the flow will reattach downstream of the nozzle.

I.1.3 Boundary Layer Growth

Initially the design study was concerned mainly with the problems arising from the large rate of sand lofting anticipated in a high speed test. The problem of boundary layer growth and

the maintenance of an undisturbed free stream flow with minimal axial and transverse pressure gradients was also undertaken. The calculations so far performed apply only to the steady state. Using by analogy Walitt's[22] results, the steady state calculation can be applied to a transient test after a time that is given approximately by $2x/u_o$, where x is the axial distance from the leading edge of the sand layer. The boundary layer thickness is calculated from

$$\frac{d\theta}{dx} = \frac{c_f}{2},$$

when θ is the momentum thickness[23] and c_f is the skin friction coefficient, with the assumption that the velocity profile is governed by the logarithmic law of the wall (Eq. 4), and that the net flux of momentum carried by the sand through the boundary layer is negligible

Casting Eq. 4 in the form

$$\frac{u_o}{u_*} = 2.5 \log_e\left(\frac{2g\frac{\delta}{\theta}}{u_*^2}\theta\right) + 9.7 \qquad (7)$$

and referring to Figure 19, with $y = \delta$ and $u = u_o$, u_o/u_* as a function of $(2g\delta/\theta)\theta/u_*^2$ may be approximated by

$$\frac{u_o}{u_*} = -0.87875\left[\log_e\left(\frac{2g\frac{\delta}{\theta}}{u_o^2}\theta\right)\right]^2 - 1.4985\log_e\left(\frac{2g\frac{\delta}{\theta}}{u_o^2}\theta\right) + 20.289 \qquad (8)$$

The ratio of the boundary layer thickness to the momentum thickness, δ/θ, was set equal to $(a+1)(a+2)/a$ (Ref 23) with a obtained by replotting Zingg's[10] data as a log-log relation. The average value of a was

3.03. Because the integral equation of Von Karman[23] was employed to determine the boundary layer thickness it is felt that the error introduced by setting δ/θ equal to a constant derived from a power law relation is small. Introducing Eq. 8 into Eq. 6 and integrating numerically, the relation between the displacement thickness, δ^*, (Ref 23) and distance along the particulate bed is obtained for various values of the free stream velocity (Figure 23). The calculation predicts a finite boundary layer thickness at the leading edge of the particulate bed, a result which arises from use of Eq. 4, which dictates that $u/u_* = 5$ at the leading edge of the boundary layer. Measurements made at culmination of the program show $u/u_* < 5$ at some locations in the boundary layer; Eq. 4 can almost surely not be used near the leading edge of the boundary layer.

To minimize wall effects the number of particulates striking the tunnel roof should be kept as small as possible. The height of the lofted particulate layer, obtained by calculating particle trajectories in the boundary layer, is plotted in Figure 24 as a function of free stream velocity. Figure 24 applies to a station located 21 ft from the leading edge of a particulate bed containing sand grains 0.25 mm in diameter. The height to which a particulate is lofted increases as the leading edge of the particulate bed is approached. The rate of decrease of lofted height with increasing axial position decreases as the wind velocity increases. At a low velocity, such as 44 fps, the lofted height is approximately $\frac{1}{2}$ the value of $u_*^2/2g$, but at high velocities, such as 350 to 430 fps, the lofted height is only 1/20 to 1/25 the value of $u_*^2/2g$.

The axial increase in the displacement thickness will cause a corresponding increase in the free stream velocity. A first order approximation for the increase in the free stream velocity relative

to the velocity at the tunnel entrance for various tunnel heights and flow velocities is plotted in Figures 25 and 26. A good simulation of atmospheric effects requires that the increase in the flow velocity at any axial position in the wind tunnel be kept to a minimum. However, the flow velocity increases rapidly with initial velocity for a fixed tunnel height; whereas for u_o = 44 fps at the tunnel inlet, a tunnel 18" high and 20' long will, according to the calculation, limit the increase in flow velocity to about 20%, a tunnel more than 20 ft high is needed to limit the increase in flow velocity to 20% when u_o = 352 fps.

The great disparity between the relatively low lofting rates determined experimentally and the upper bound provided by the theoretical calculations indicates that much remains to be learned about boundary layers with particulate lofting.

APPENDIX II

TUNNEL FLOW CHARACTERISTICS

The relationship between the time for the tunnel to reach steady state gas flow conditions and the rate of depletion of the particulate bed was crucial for the conduct of these experiments. The rise time of the tunnel free stream velocity was fairly long (Figure 27), yet the relatively low lofting rates allowed the tests to be carried out without modification of the cross wind facility. The test time for the purpose of calculating lofting rates was determined with the free stream velocity arbitrarily set equal to 95% of maximum free stream velocity, a convention that tended to overestimate the lofting rate.

REFERENCES

1. Owen, P.R., "Saltation of Uniform Grains in Air," J. Fluid Mechanics, 20, Pt. 2, pp. 225-242 (1964).

2. Gumprecht, R.O. and Sliepcevich, C.M., "Scattering of Light by Large Spherical Particles," J. Phys. Chem., 57, p. 192 (1953).

3. Lord Rayleigh, quoted in Reference 2.

4. Middleton, W., Vision Through the Atmosphere, Univ. of Toronto Press, Toronto (1941).

5. Dussourd, J., "A Theoretical and Experimental Investigation of a Deceleration Probe for Measurement of Several Properties of a Droplet-Laden Air Stream," Sc.D Thesis, M.I.T., Dept. Mech. Eng. (October 1954).

6. Dussourd, J., ibid.

7. Owen, P.R., ibid.

8. Glenn, L. and Trulio, J., "The Lofting of Debris and Particulate Ejecta by Blast-Induced Surface Shear," Applied Theory, Inc. Report ATR-70-14-3.

9. Bagnold, R.A., "The Physics of Blown Sands and Desert Dunes," Morrow, N.Y. (1942).

10. Zingg, A.W., "Wind-Tunnel Studies of the Movement of Sedimentary Material," Proc. 5th Hydraulics Conf., Univ. of Iowa Studies in Eng., Bull., 34, III, pp. 111-135 (1953).

11. Owen, P.R., ibid.

12. Glenn, L. and Trulio, J., ibid.

13. Crocco, L., "One Dimensional Treatment of Steady Gas Dynamics," in Fundamentals of Gas Dynamics, H.W. Emmons, ed., Princeton, pp. 166-169 (1958).

14. Ahrens, M. and Spiegler, E., "Separated Flow in Overexpanded Nozzles at Low Pressure Ratios," Bull. Res. Counc. of Israel, 11C, pp. 45-55 (1962).

15. Green, L., "Flow Separation in Rocket Nozzles," ARS Journal, pp. 34-35 (Jan-Feb. 1953).

16. Scheller, K. and Bierlein, J., "Some Experiments on Flow Separation in Rocket Nozzles," ARS Journal, pp. 28-32,40 (Jan-Feb 1953).

17. Summerfield, M., Foster, C., and Swan, W., "Flow Separation in Overexpanded Supersonic Exhaust Nozzles," Jet Propulsion, pp. 319-321 (Sept-Oct 1954).

18. Bach, L. and Cuffel, R., "Detection of Oblique Shocks in a Conical Nozzle with a Circular-Arc Throat," AIAA J., 4, No. 12, pp. 2219-2221 (Dec. 1966).

19. Crocco, L., ibid.

20. Harp, J. and Haas, R., private communication.

21. Harp, J., private communication.

22. Walitt, L., Niles, W., and Trulio, J., "Numerical Calculation of Viscous Compressible Fluid Flow Over a Flat Plate and Step Geometry," NASA CR-1466 (Feb. 1970).

23. Schlichting, H., Boundary Layer Theory, McGraw-Hill New York, 1960.

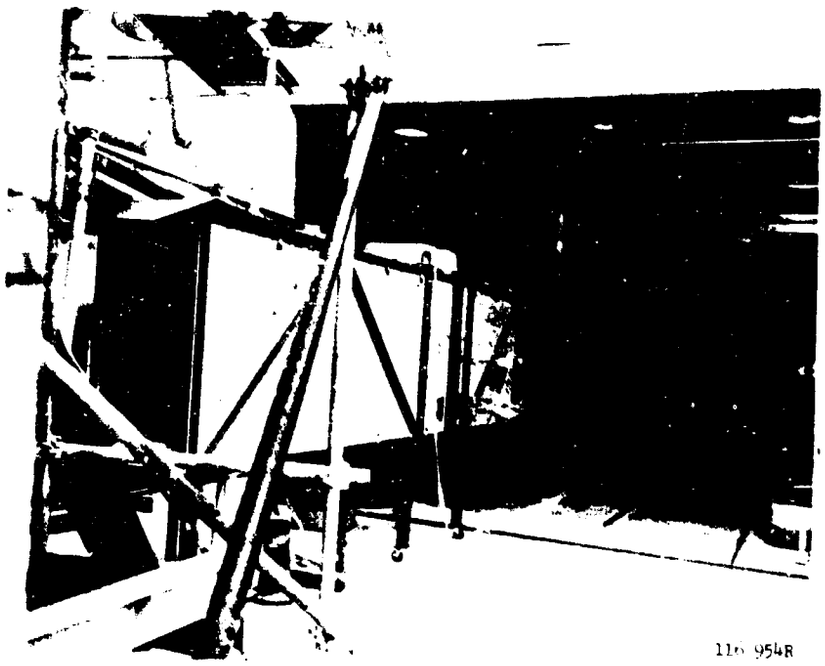

Figure 1. Lofting Tunnel.

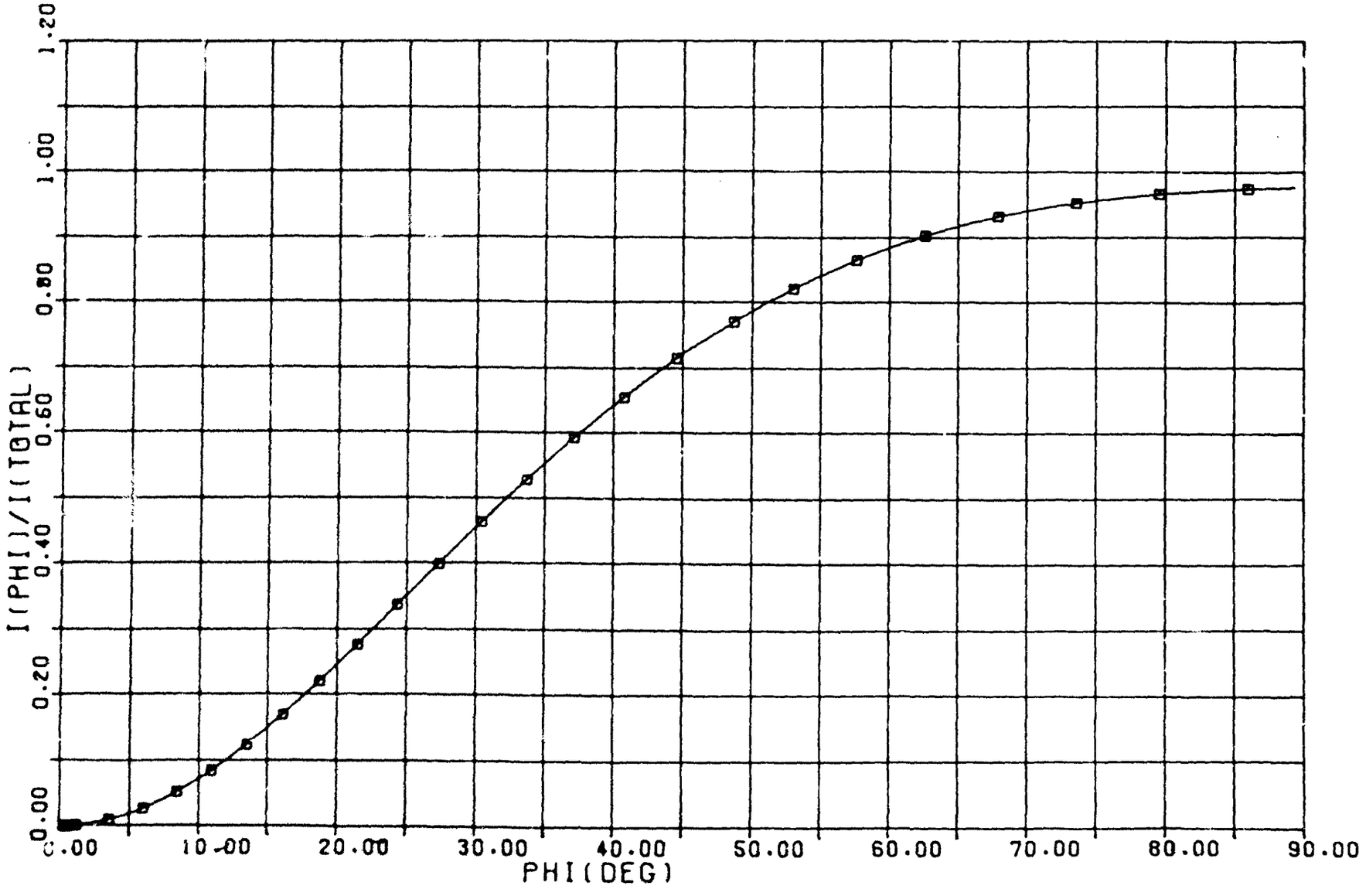

Figure 2a. Fraction of Refracted and Reflected Light Lying Within a Cone of Half Angle θ.

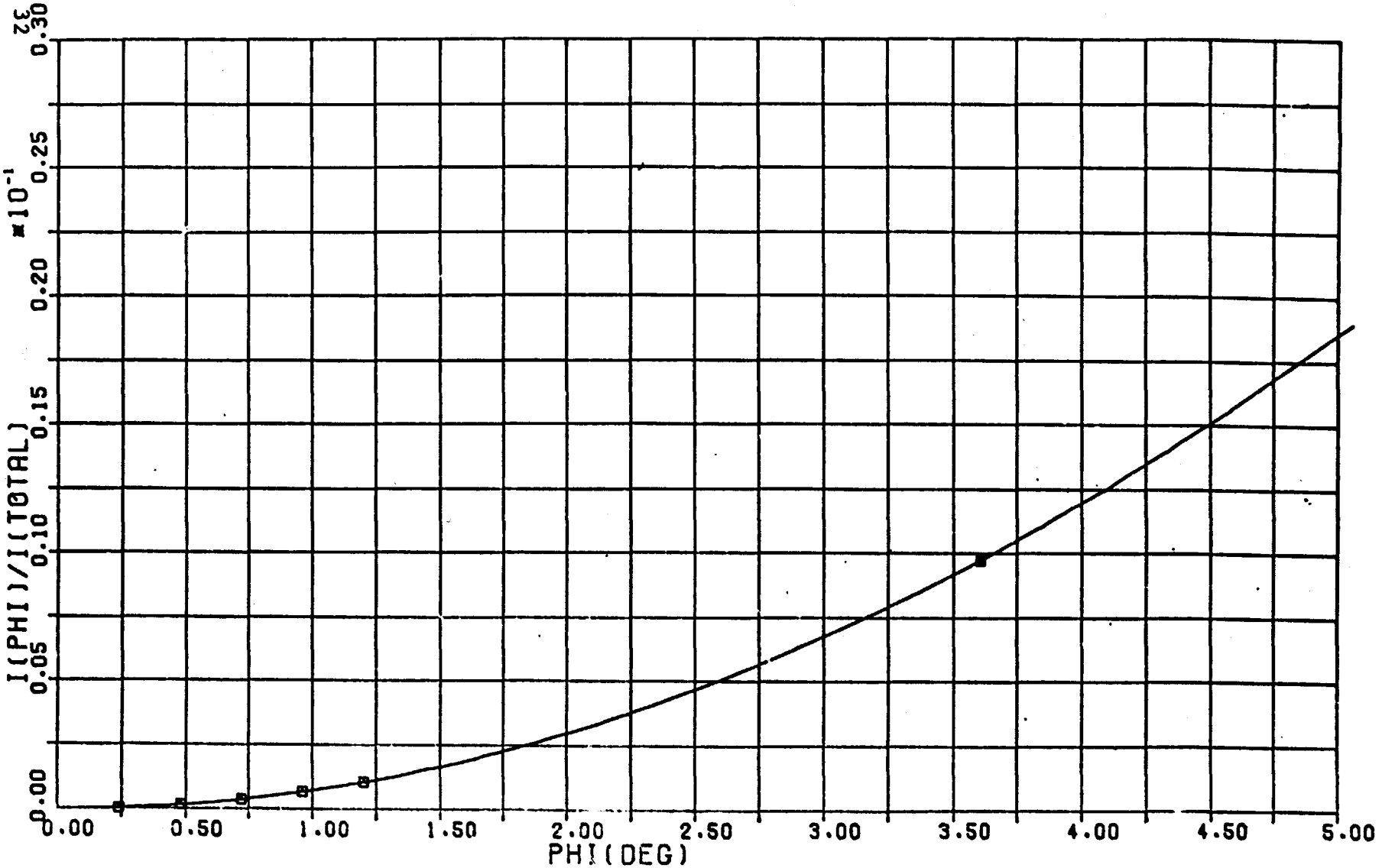

Figure 21. Fraction of Refracted and Reflected Light Lying Within a Cone of Half Angle θ.

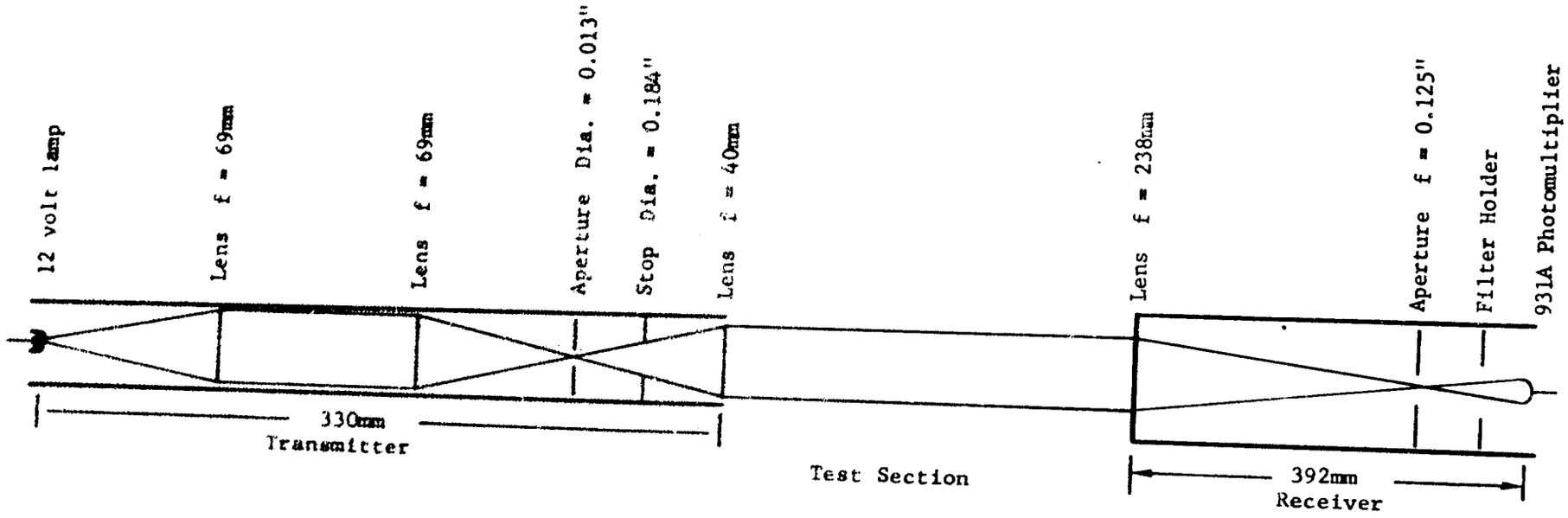

Figure 3. Setup for Light Extinction Measurement.
Transmitter Tube O.D. = 5/8".
Receiver Tube O.D. = 3/4".

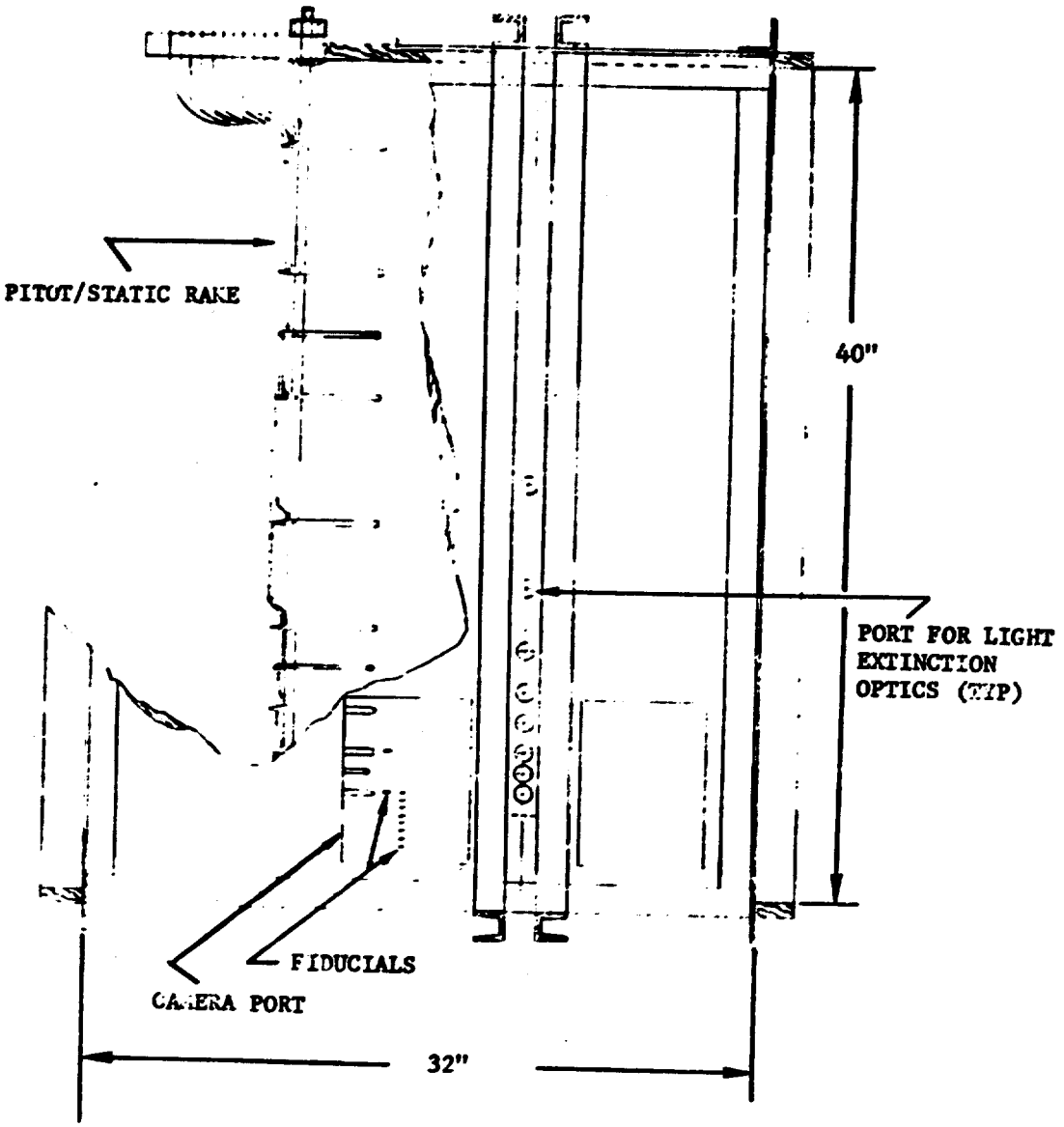

Figure 4. Diagnostics Section.

Figure 5. Wind Tunnel Looking Upstream Showing Pitot/Static Rake and Camera Ports.

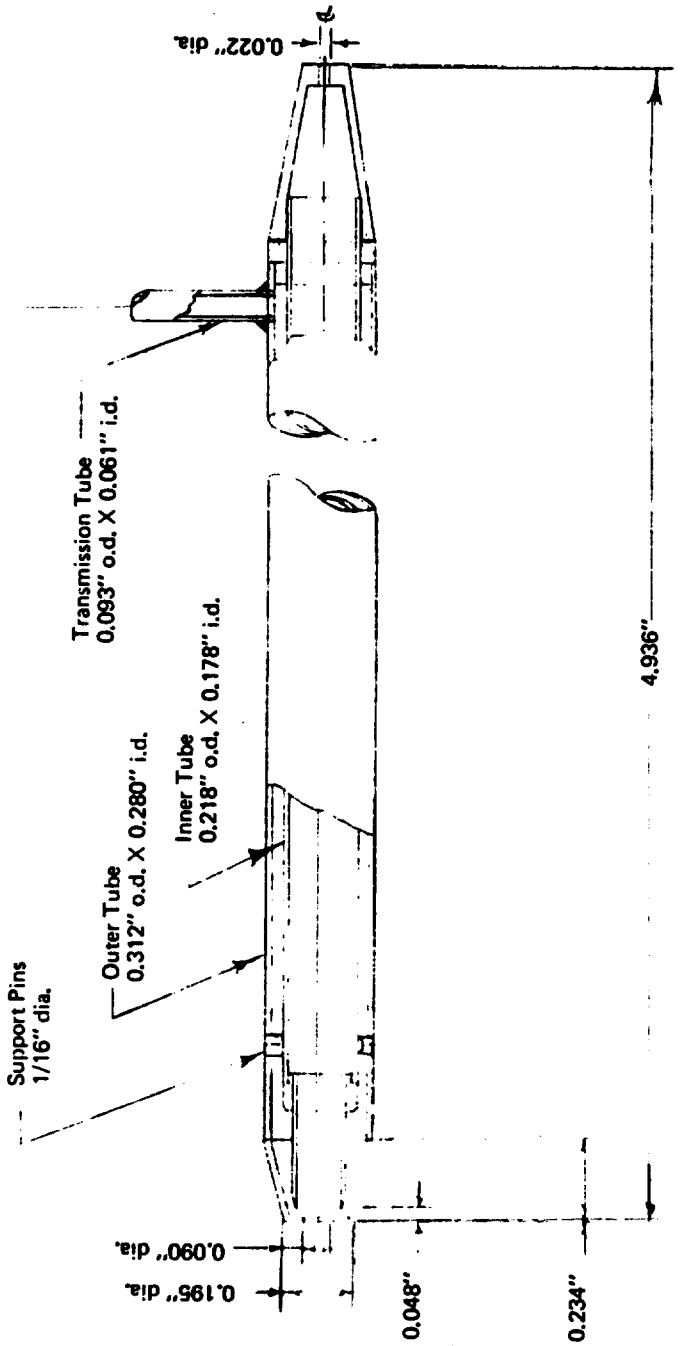

Figure 6. Coaxial Pitot Tube.

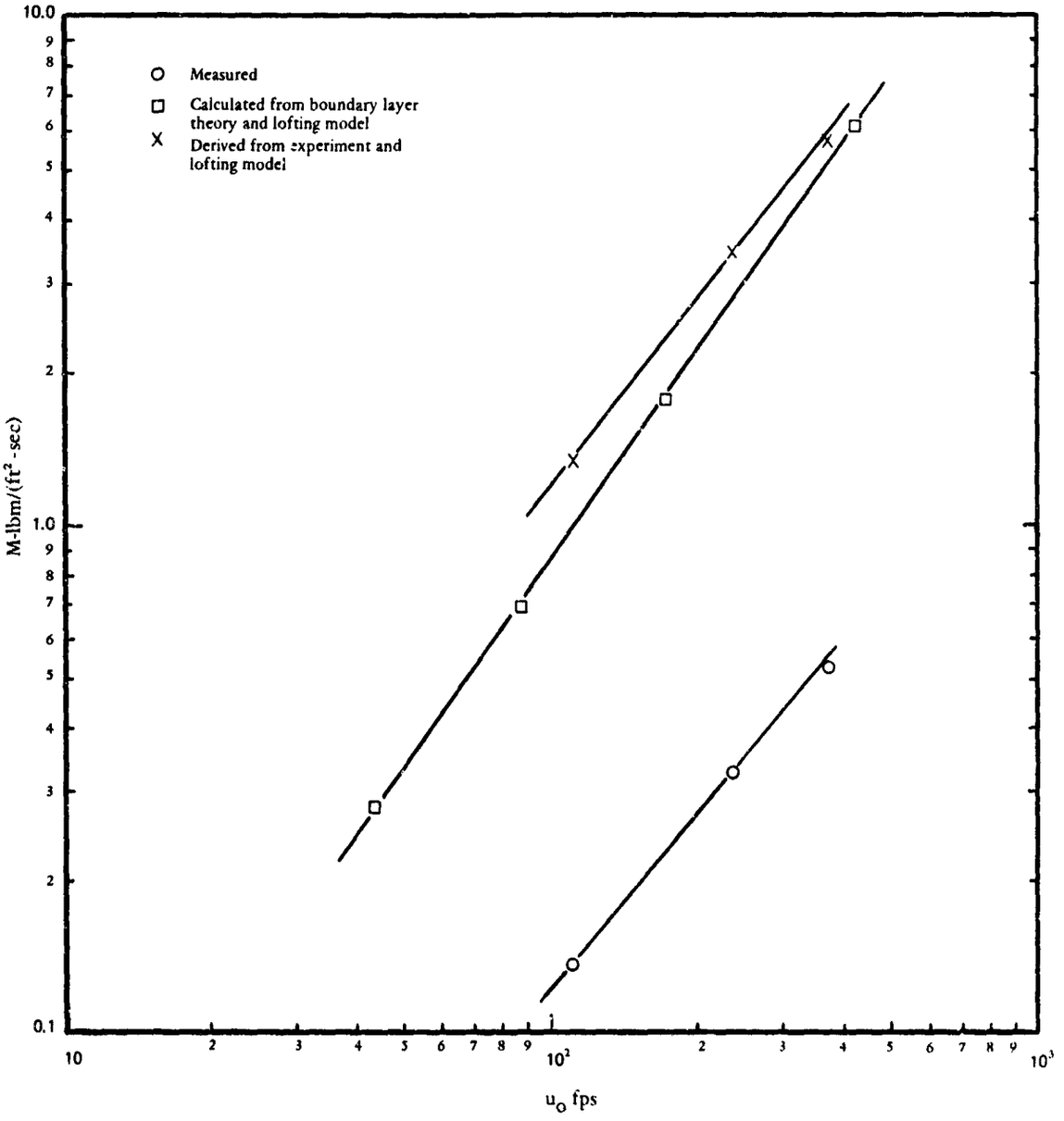

Figure 7. Lofted Mass at Fixed Position in Boundary Layer vs. Free Stream Wind Speed. Test Bed Composed of AFS 50-70 Ottawa Silica Testing Sand. Mean Diameter of Particulates: 0.25 mm.

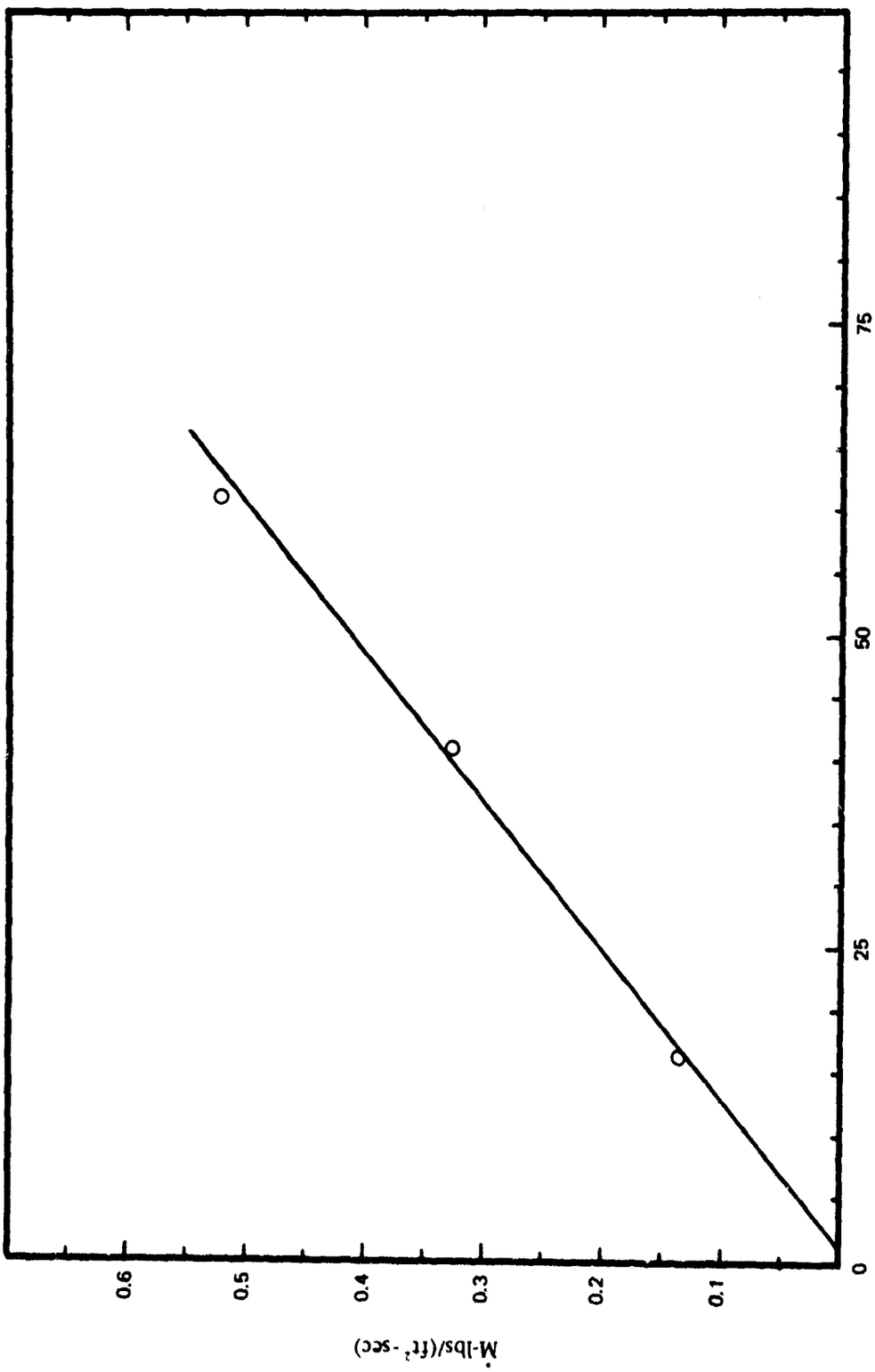

Figure 8. Lofted Mass vs. Shear Stress Velocity.

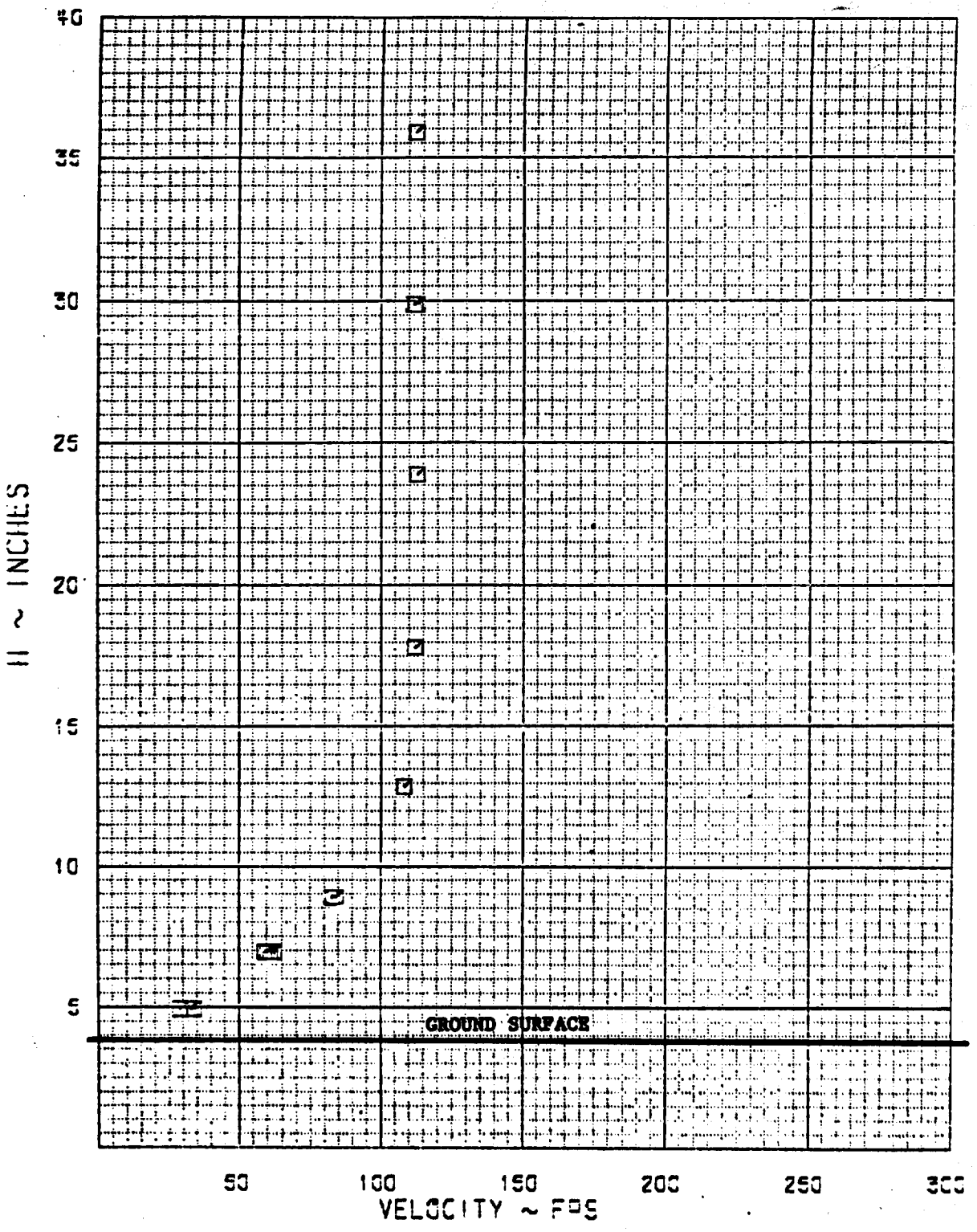

Figure 9. Boundary Layer Particulate Lofting Test u_o = 111.8 fps.

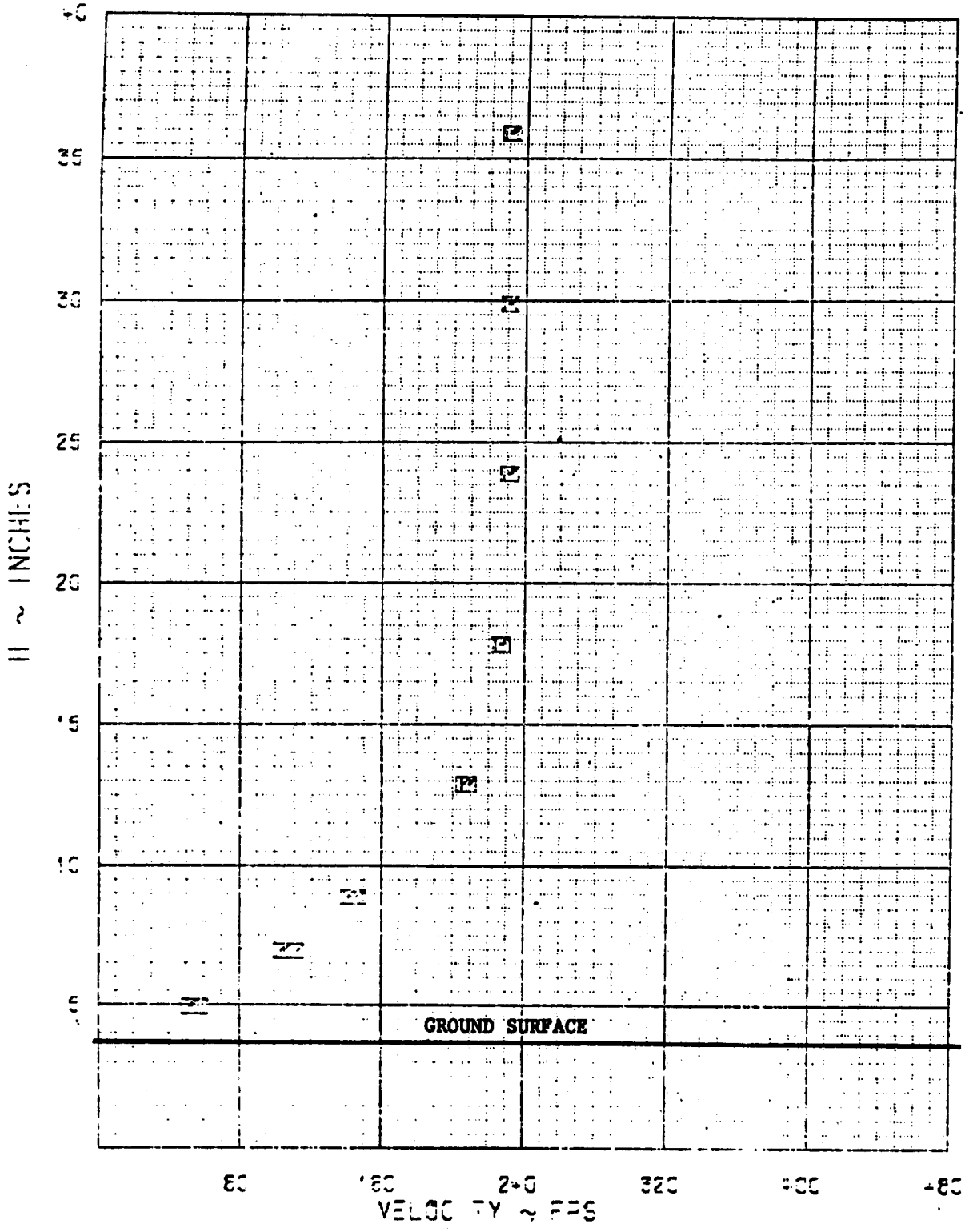

Figure 10. Boundary Layer Particulate Lofting Test, u = 237.8 fps.

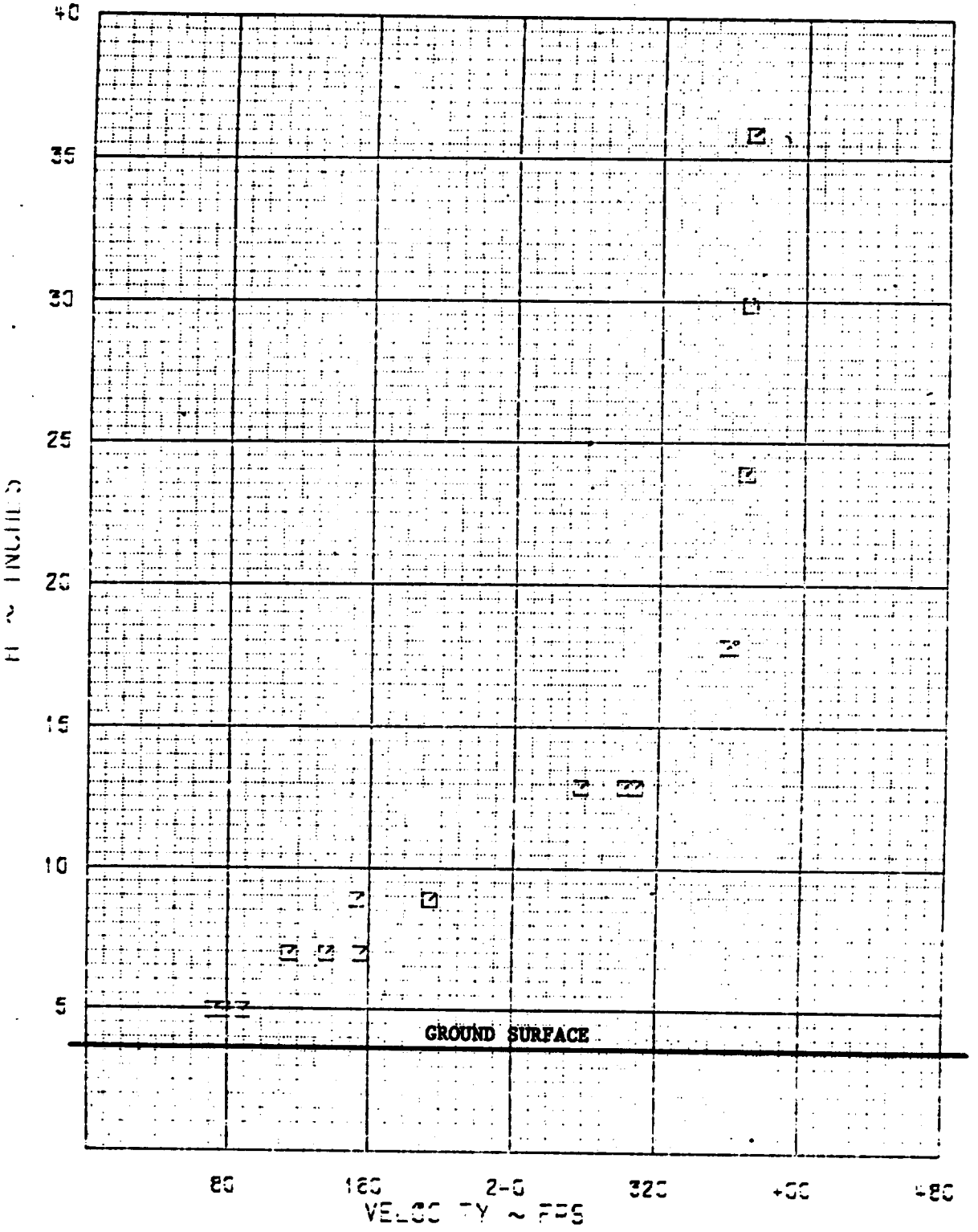

Figure 11. Boundary Layer Particulate Lofting Test, u_o = 376.3 fps.

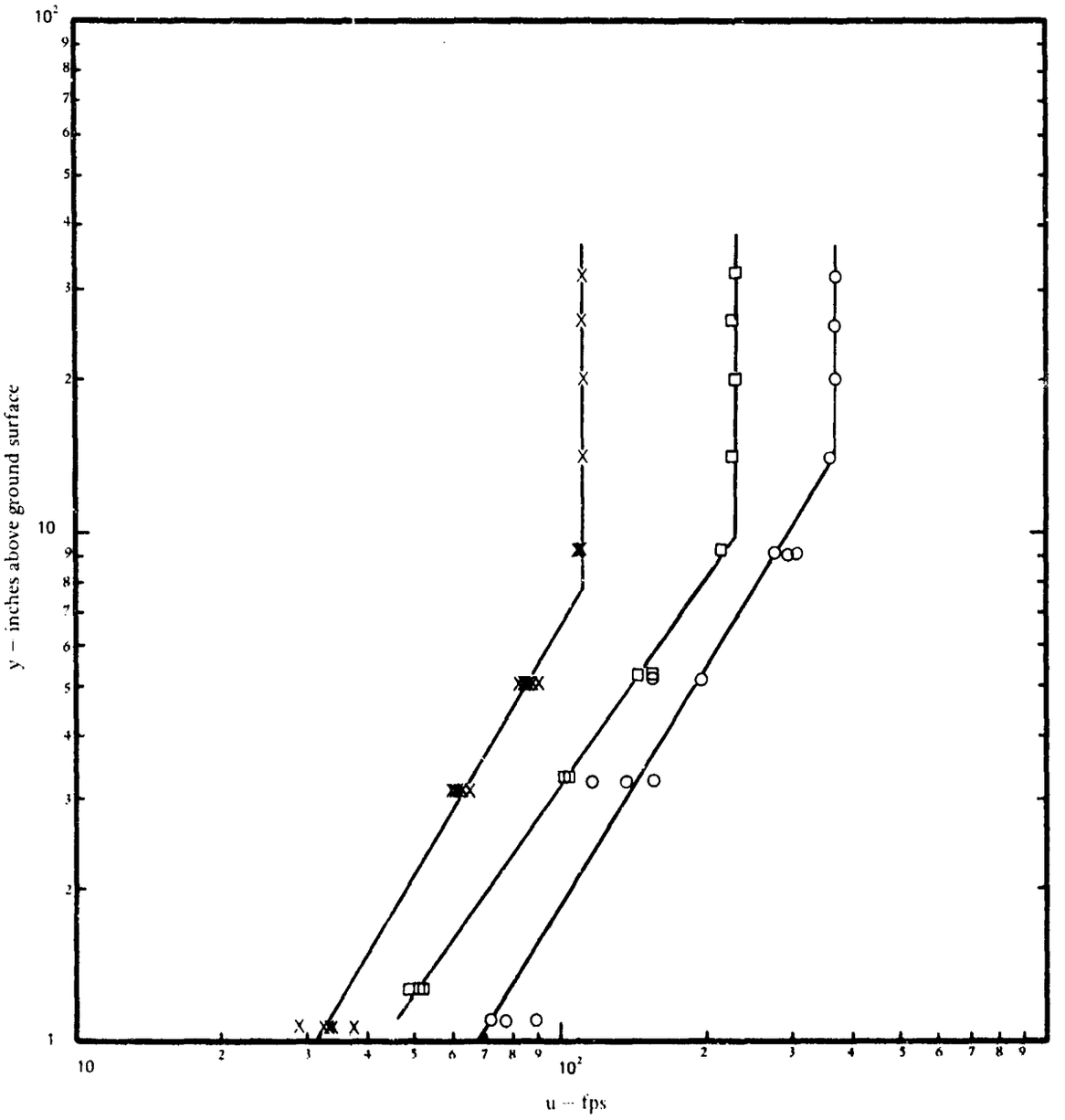

Figure 12. Wind Velocity Profile with Particulate Lofting.

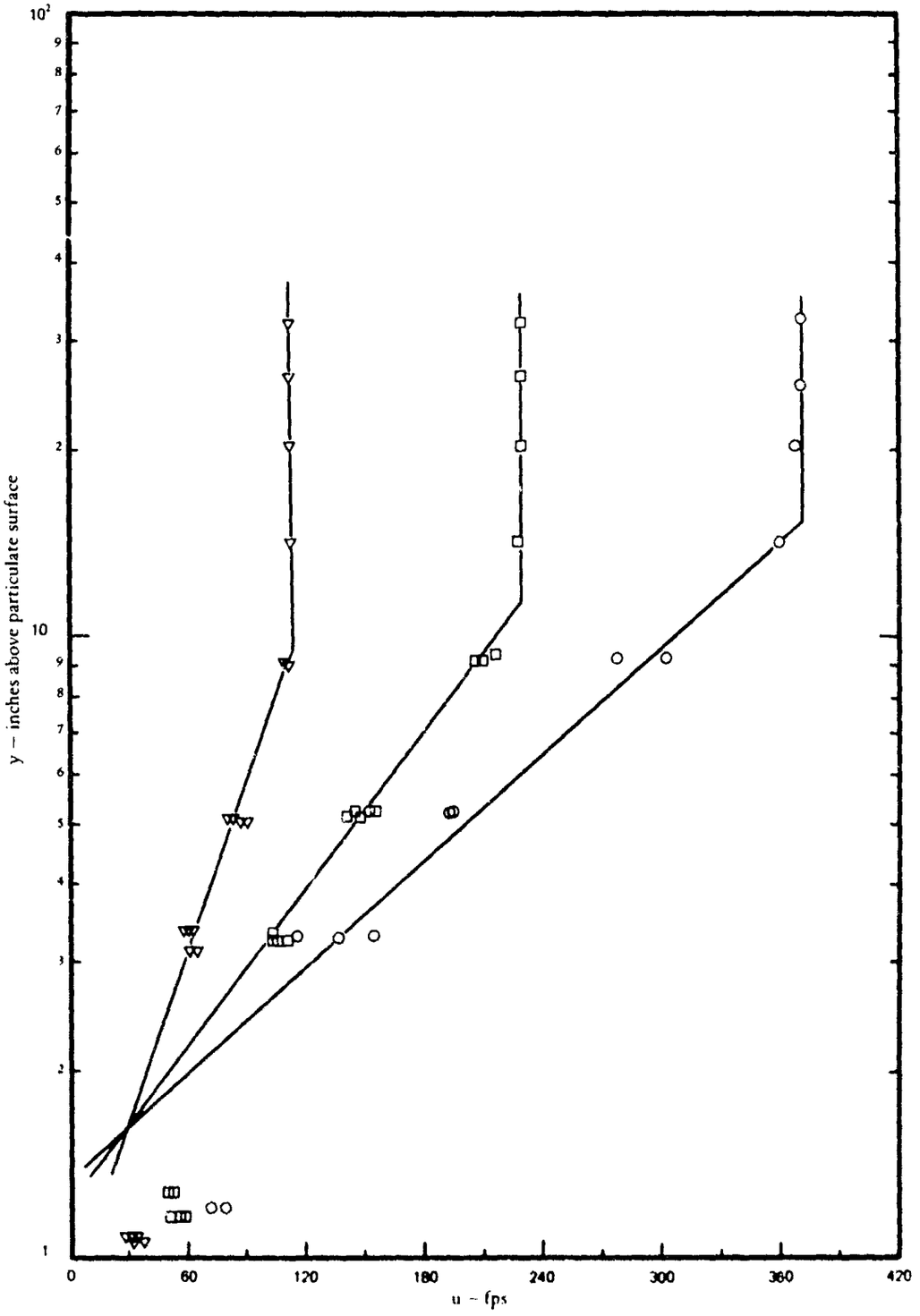

Figure 13. Law for Flow Past a Wall with Particulate Lofting.

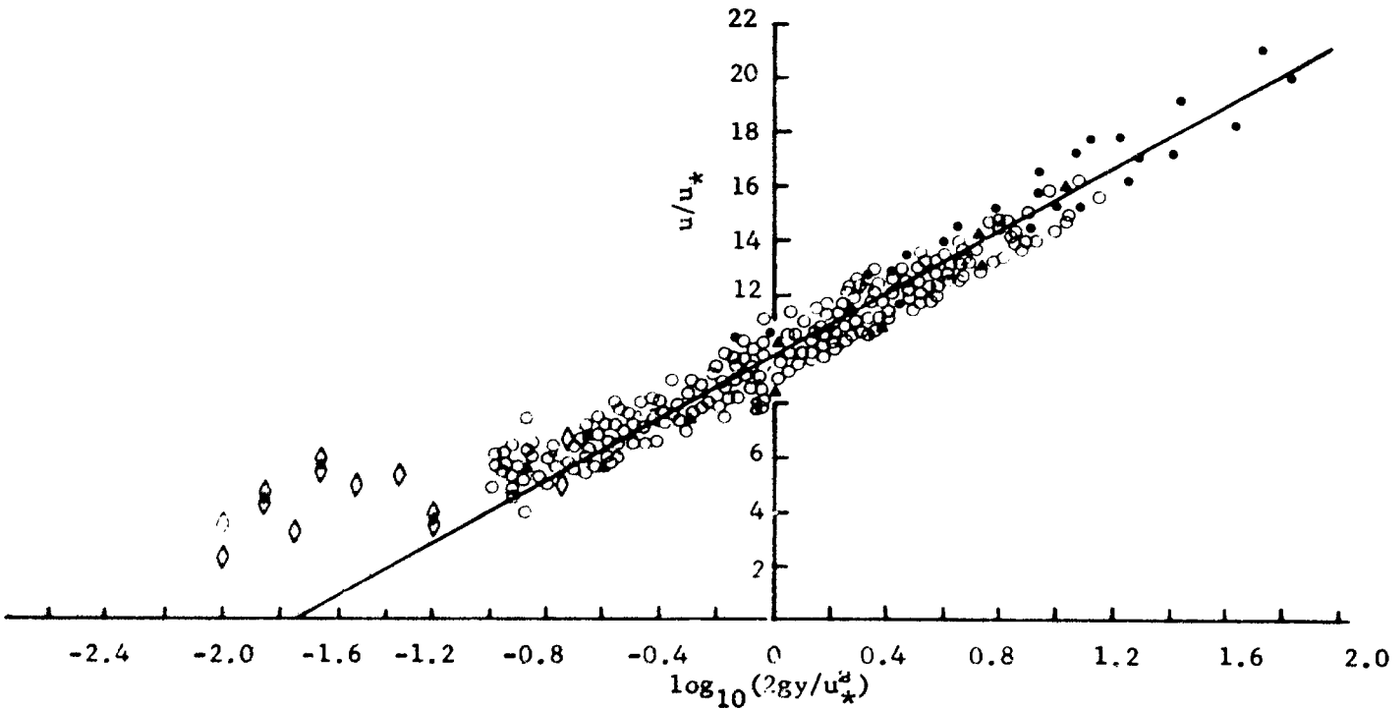

Figure 14. Wind Velocity Profile Outside the Saltation Layer.
Uniform Sand: ○ Zingg (1953)
▲ Bagnold (1941)
} Reference 1
Non-uniform Soil: ● Chepil (1945a,b,c)
Uniform Sand: ◊ Hartenbaum (1971)

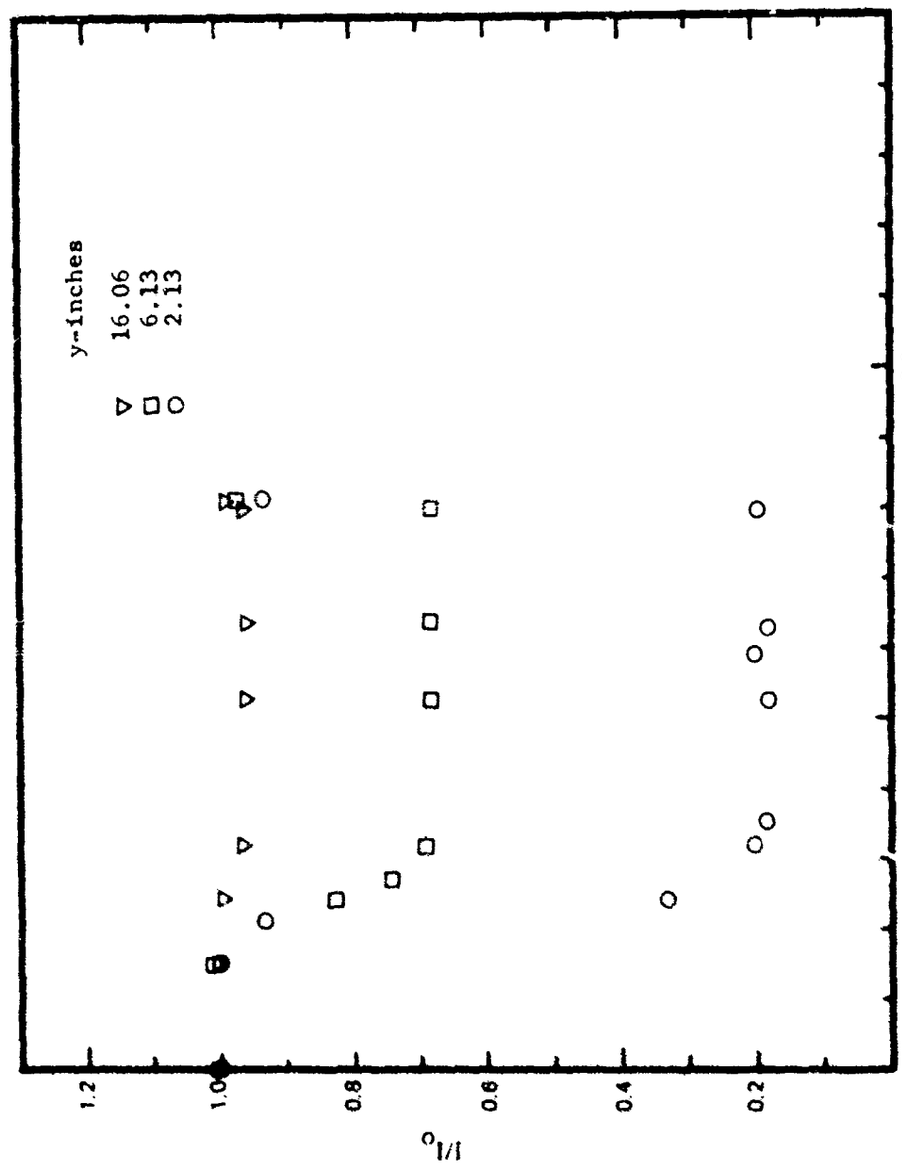

Figure 15. Detected Light Intensity vs. Time, u_o = 111.8 fps.

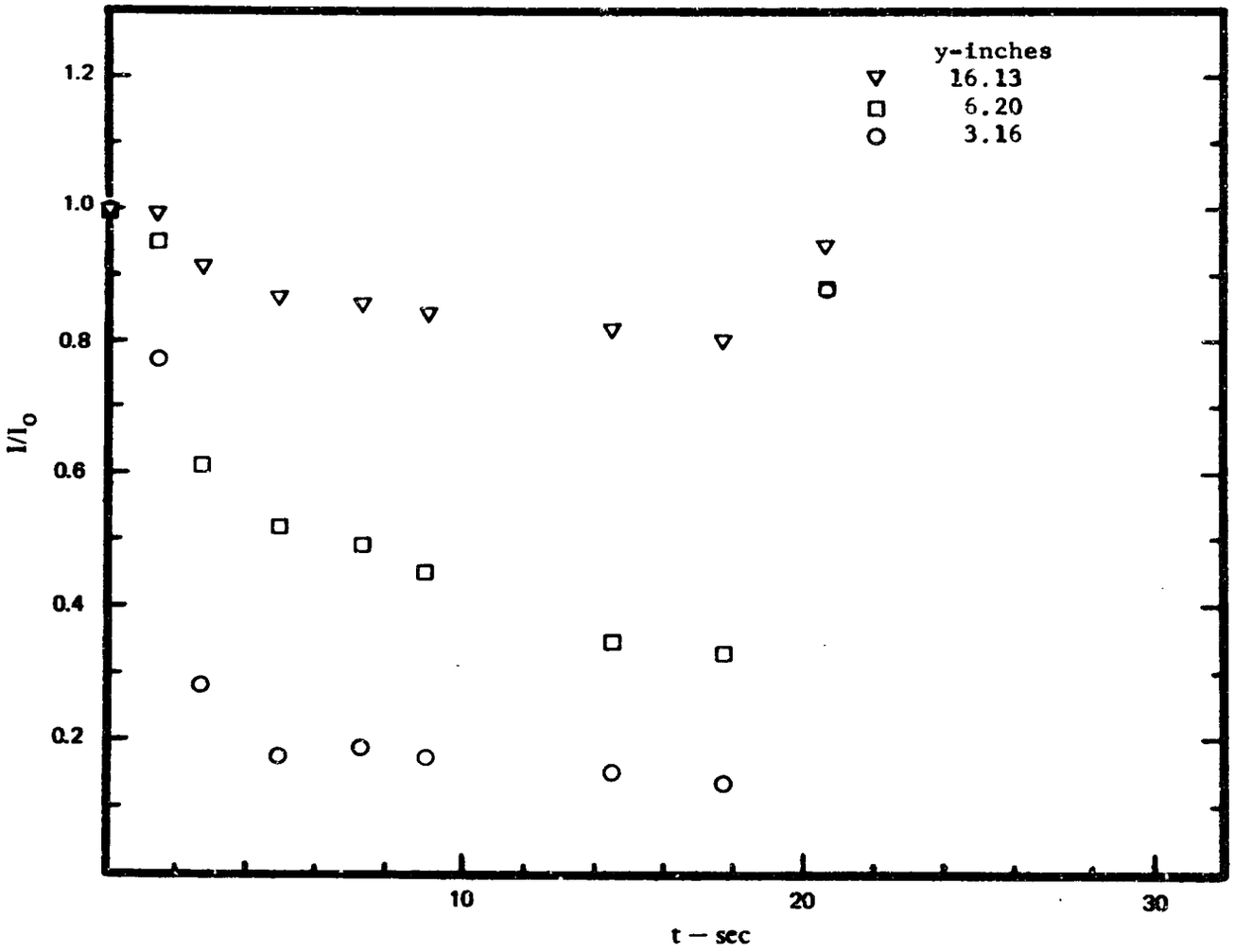

Figure 16. Detected Light Intensity vs. Time, u_o = 237.8 fps.

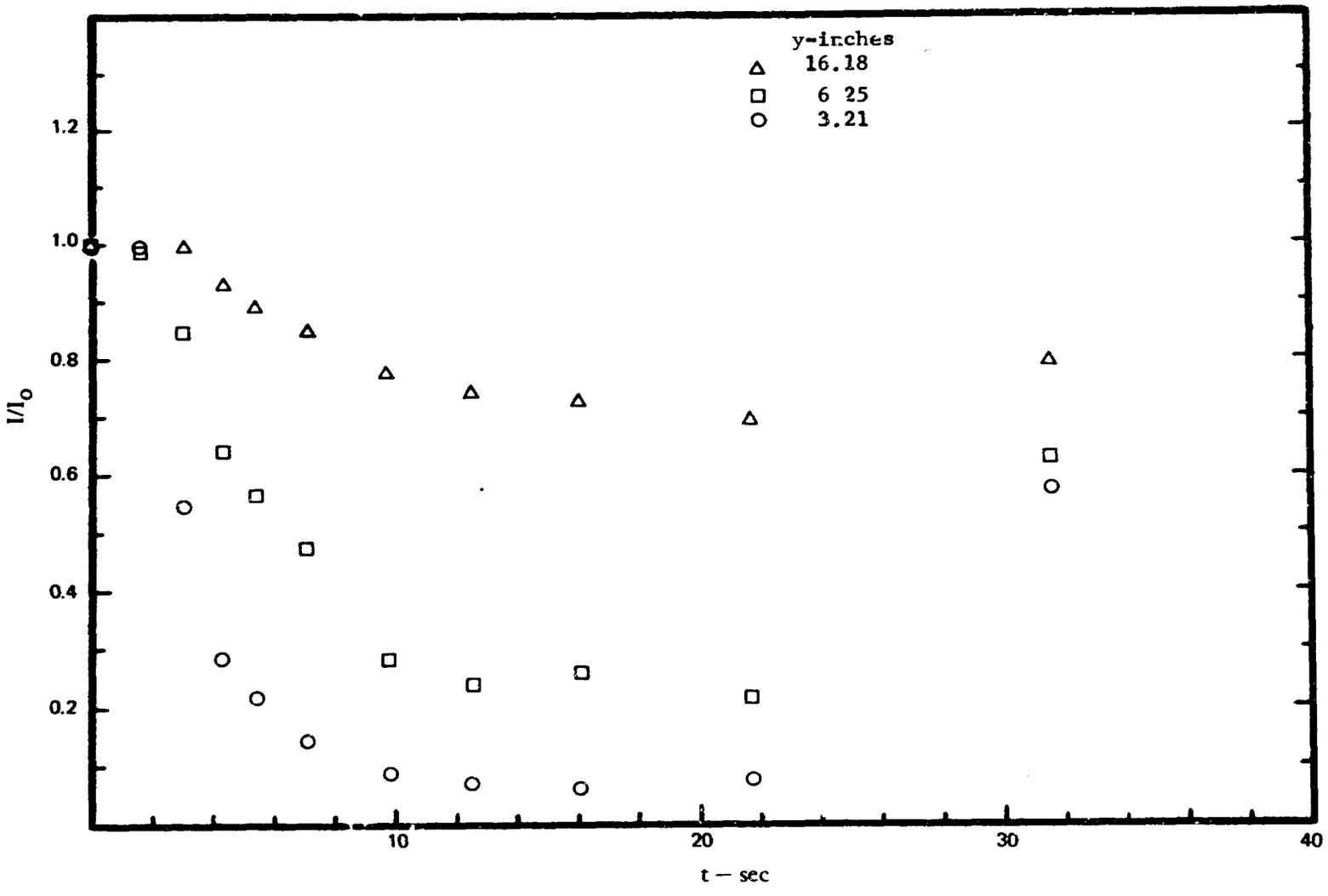

Figure 17. Detected Light Intensity vs. Time, u_o = 376.3 fps.

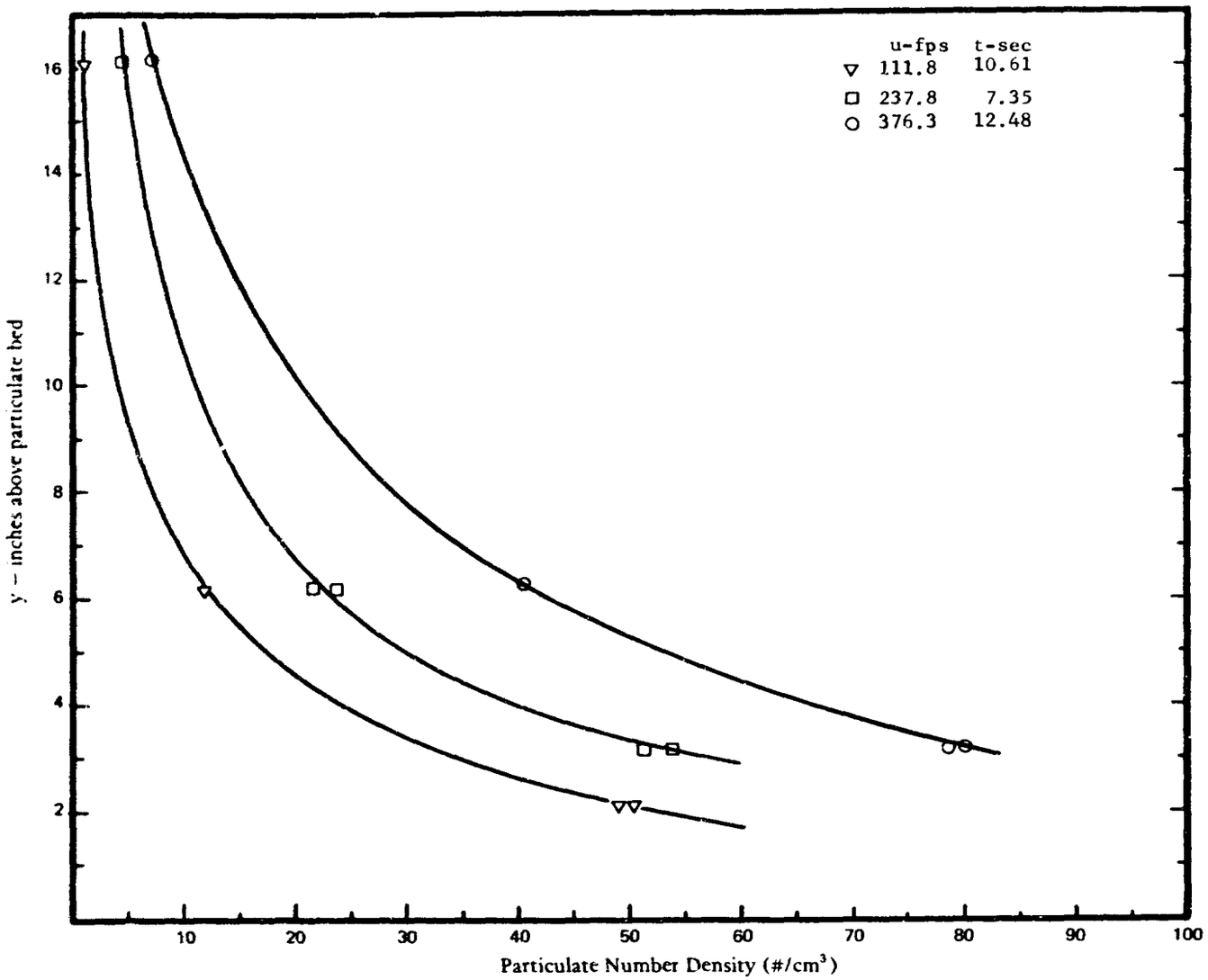

Figure 18. Density of Lofted Particulates. Mean Diameter of Particulates: 0.25 mm.

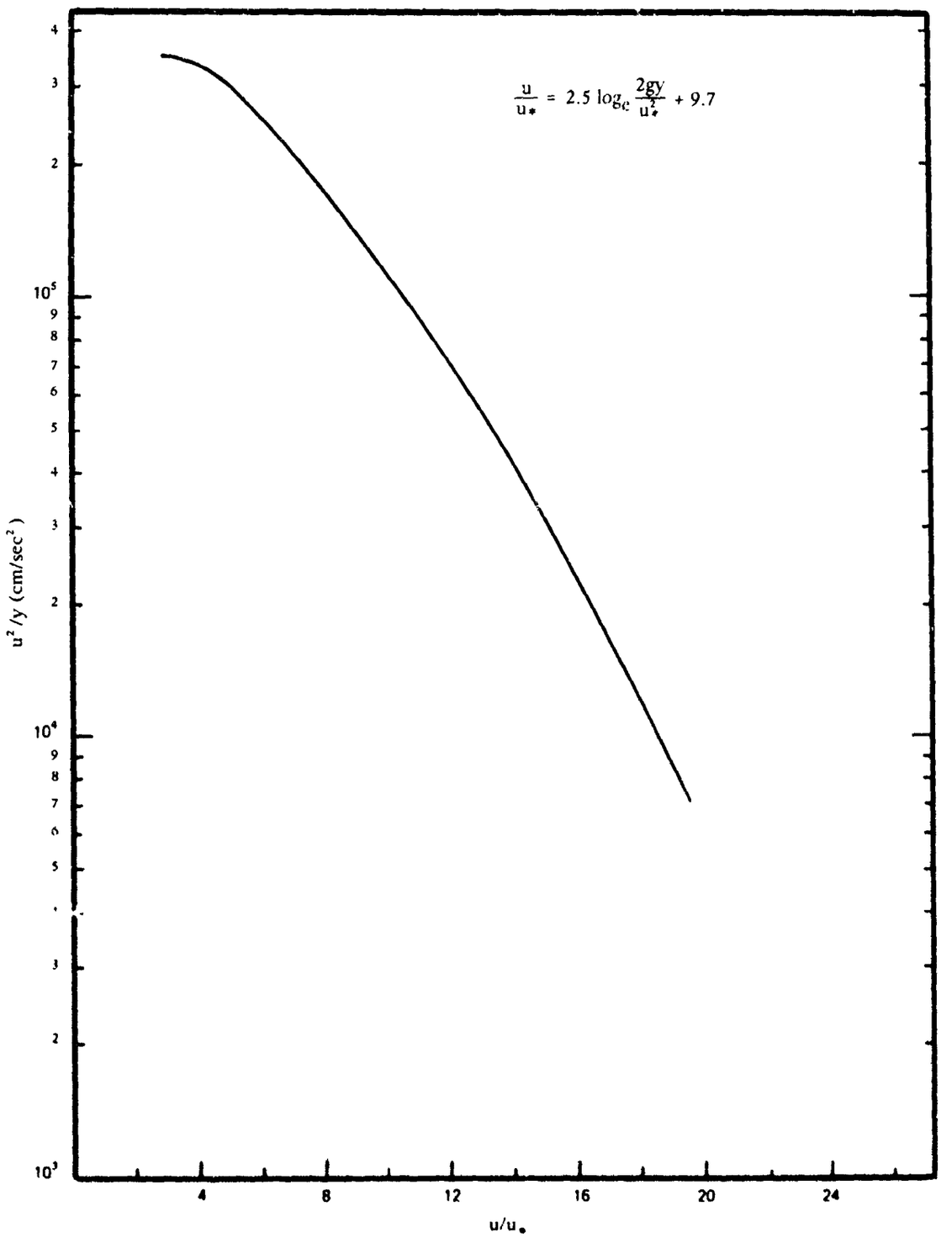

Figure 19. Velocity Wall Law for Turbulent Flow with Particulates from Owen's Relation.

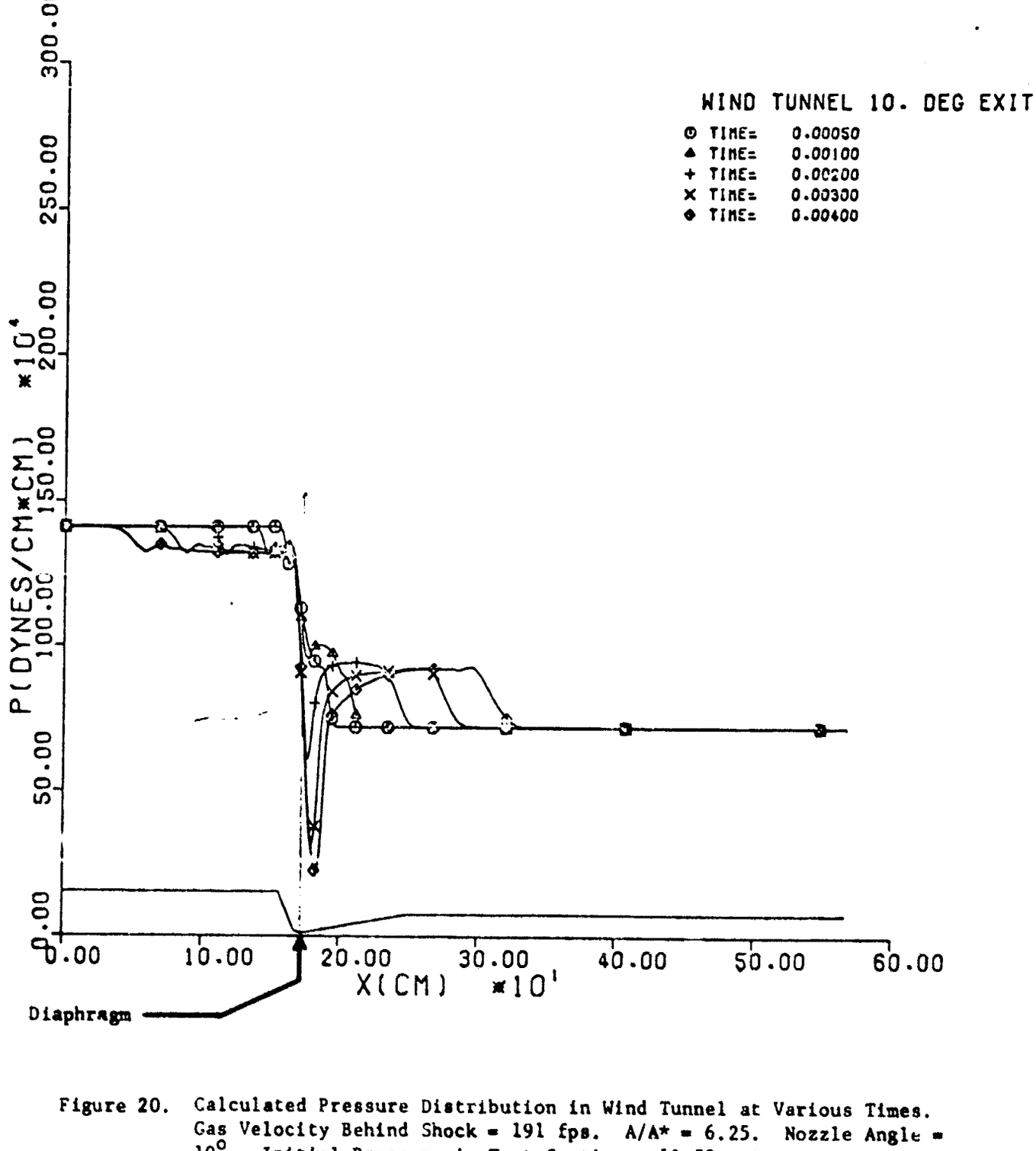

Figure 20. Calculated Pressure Distribution in Wind Tunnel at Various Times. Gas Velocity Behind Shock = 191 fps. $A/A^* = 6.25$. Nozzle Angle = 10°. Initial Pressure in Test Section = 10.58 psia.

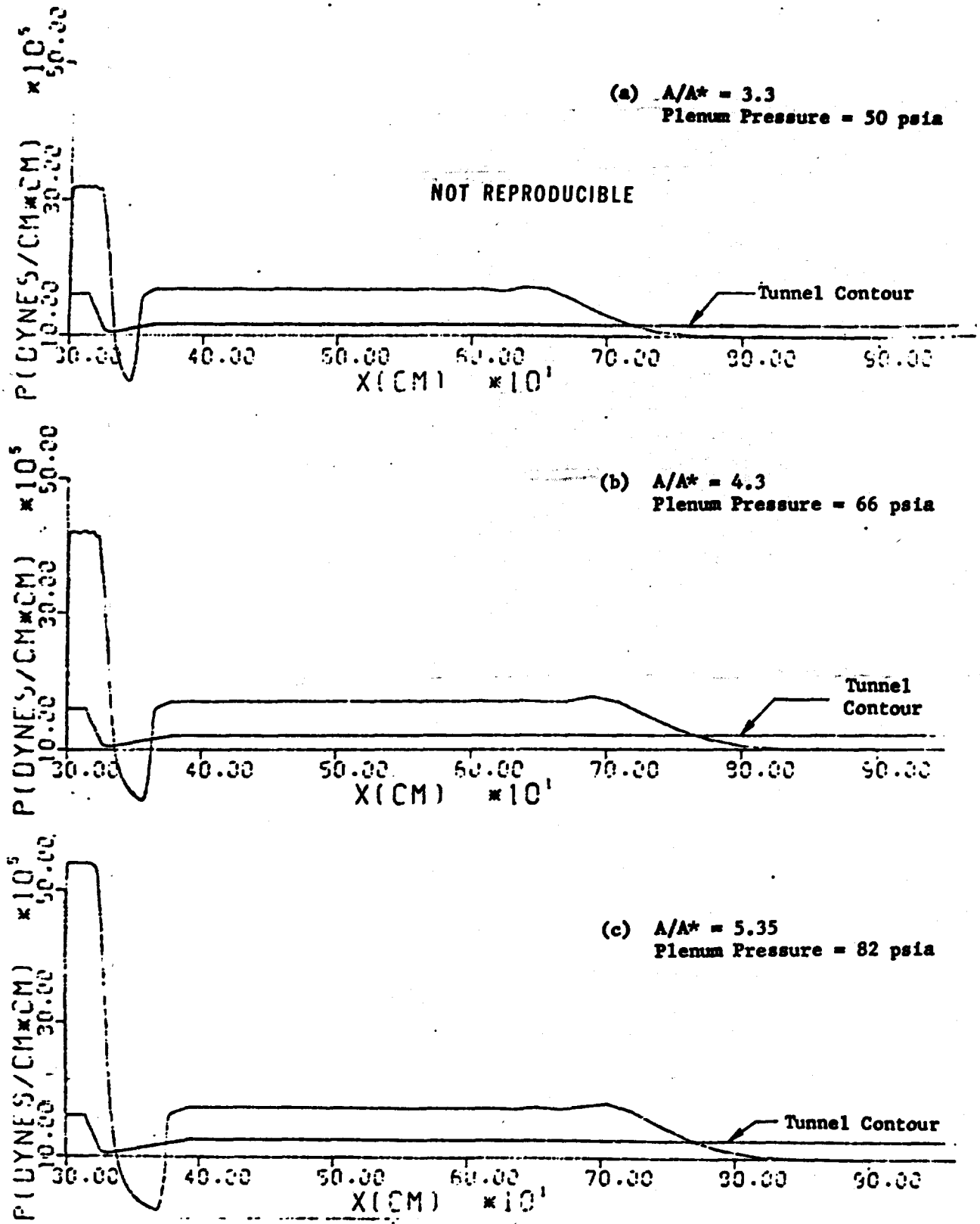

Figure 21. Calculated Pressure Distribution in Wind Tunnel at 10 millisec. Nozzle Angle = 10°. Initial Pressure in Test Section = 14.7 psia.

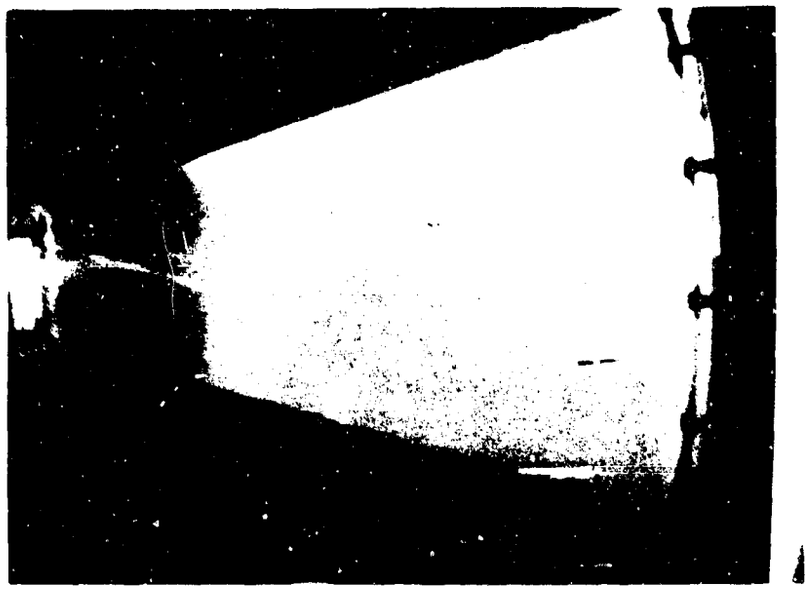

(a) Self Luminous Photograph of Flow in Convergent – Divergent Nozzle; Luminosity from $NaHCO_3$ Seed

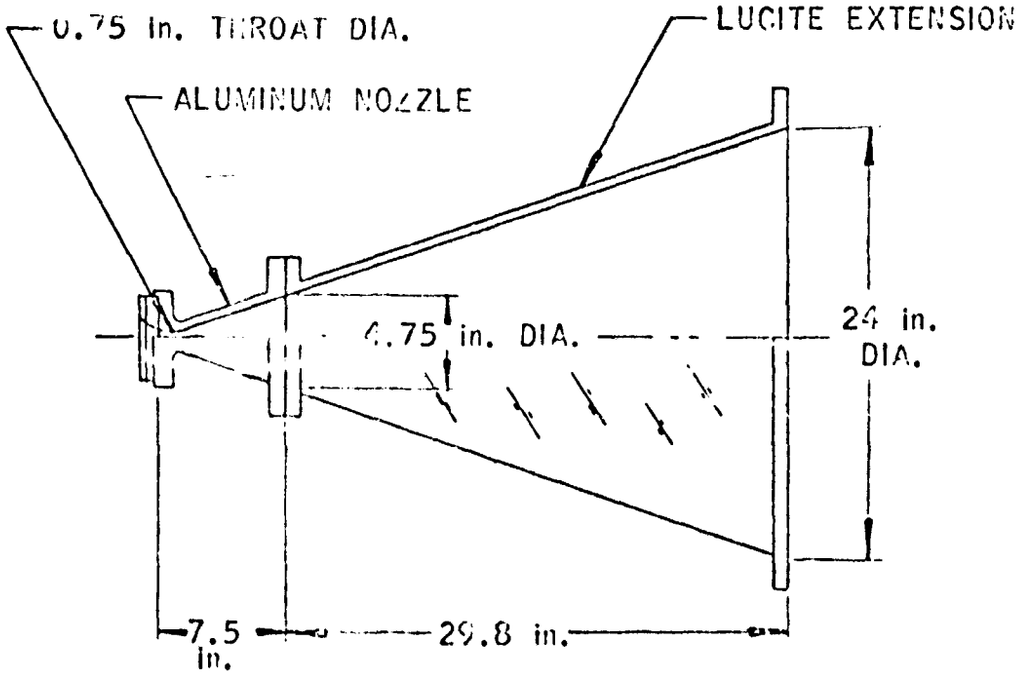

(b) Marquardt Nozzle (Over-all A/A* = 1000)

Figure 22. Normal Shock in Supersonic Nozzle of Hot Shot Tunnel.

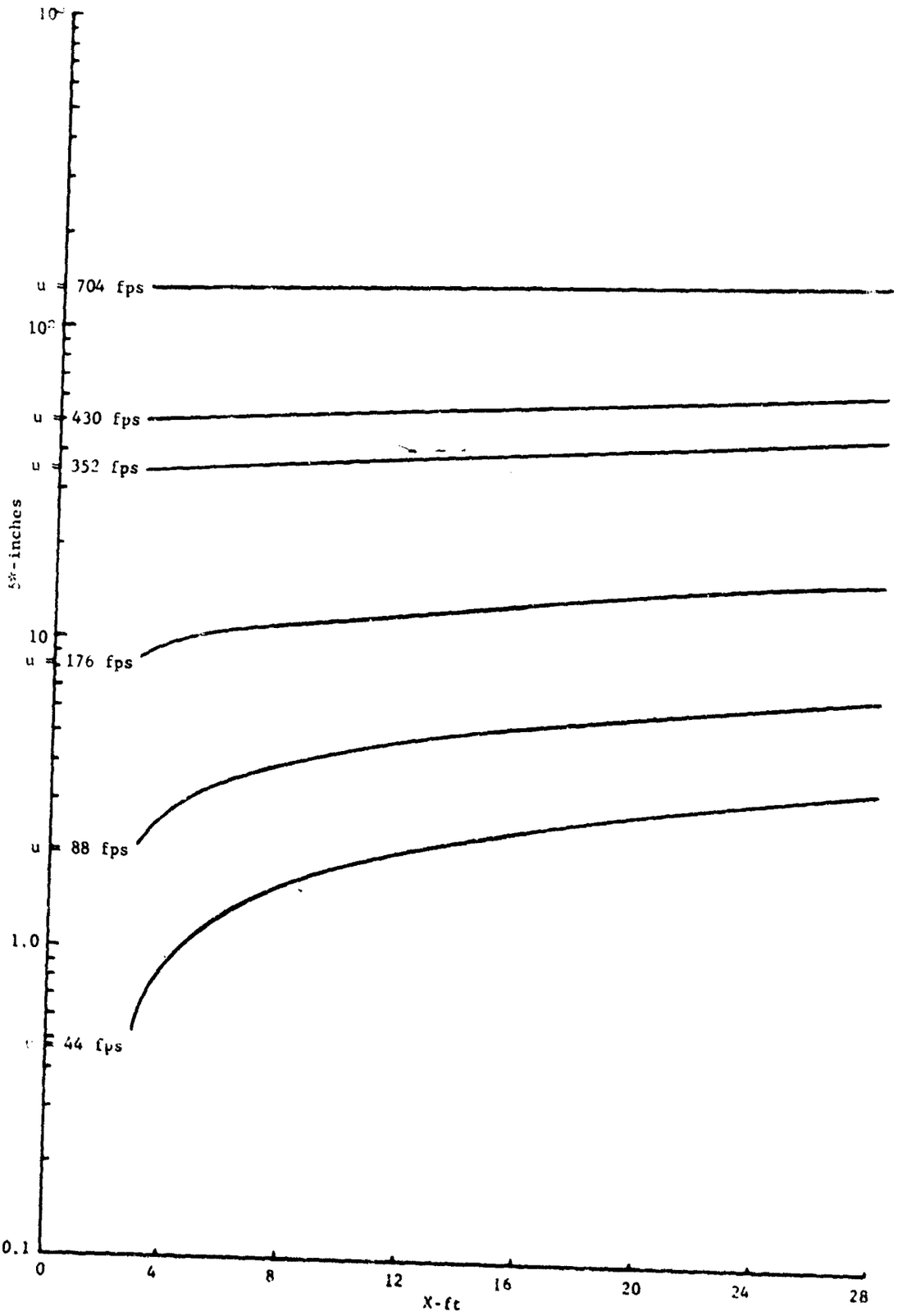

Figure 23. Calculated Displacement Thickness (δ^*) Variation Along a Flat Plate Immersed in a Saltating Flow Saltation Layer Extends from $X \geq 3$ ft. c_f Based on Owen's Relation.

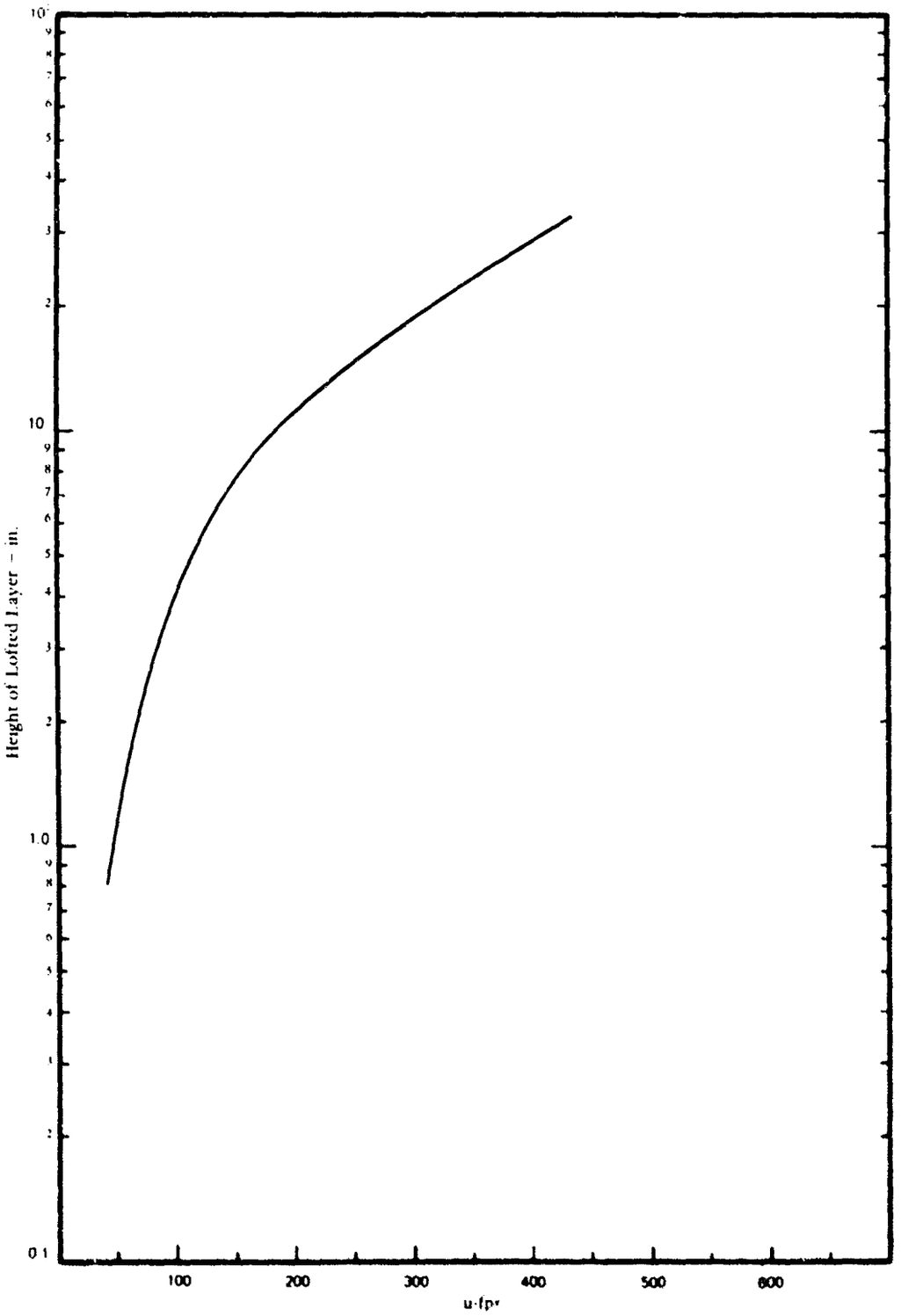

Figure 24. Calculated Height of Lofted Layer vs Free Stream Velocity at a Station 21 ft From Leading Edge of Particulate Bed. Diameter of Particulate - 0.25 mm.

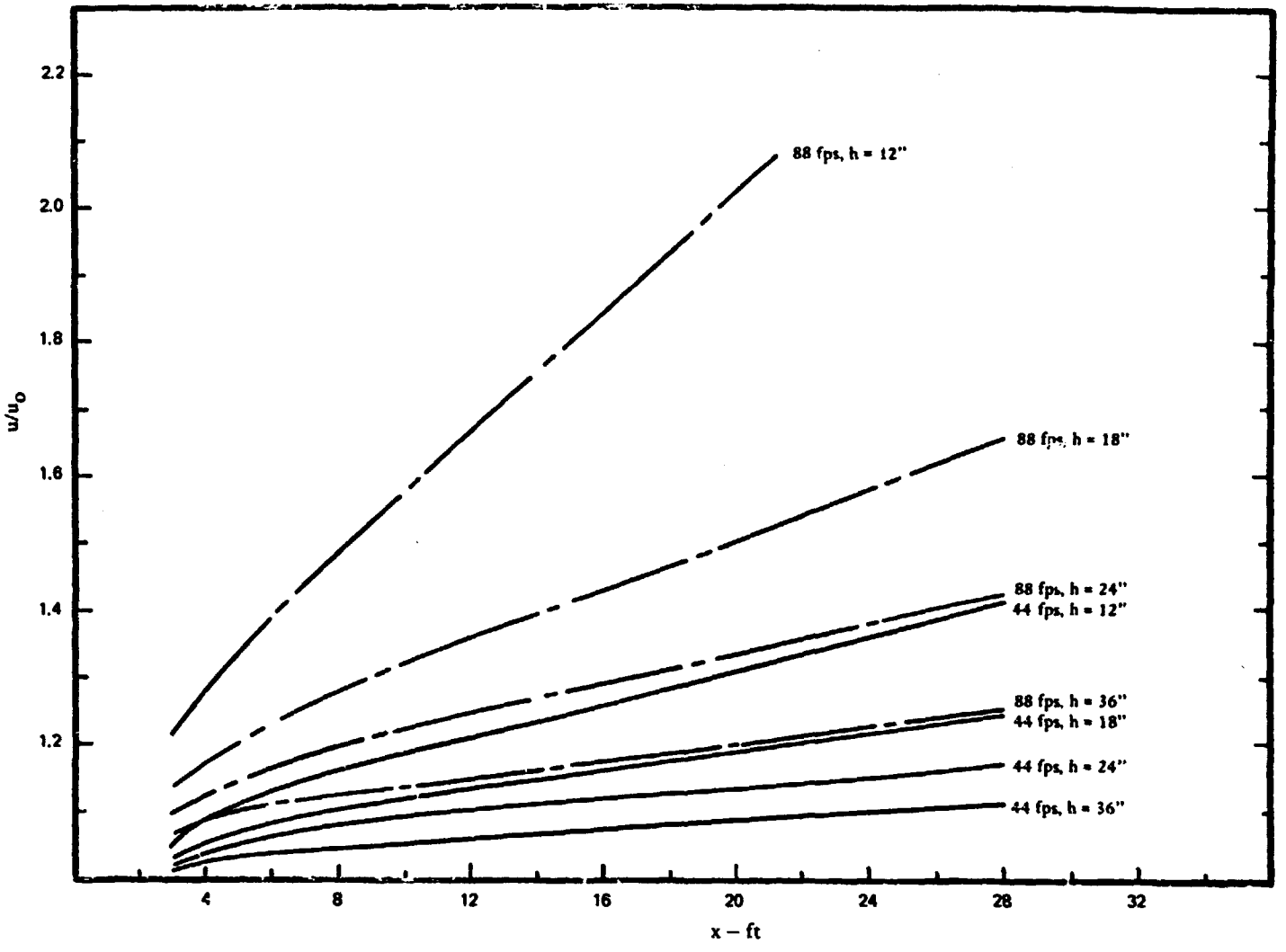

Figure 25. Calculated Relative Increase in Flow Velocity with Distance Along Particle Bed for Fixed Area Test Section with Initial Velocity and Tunnel Height as Parameters.

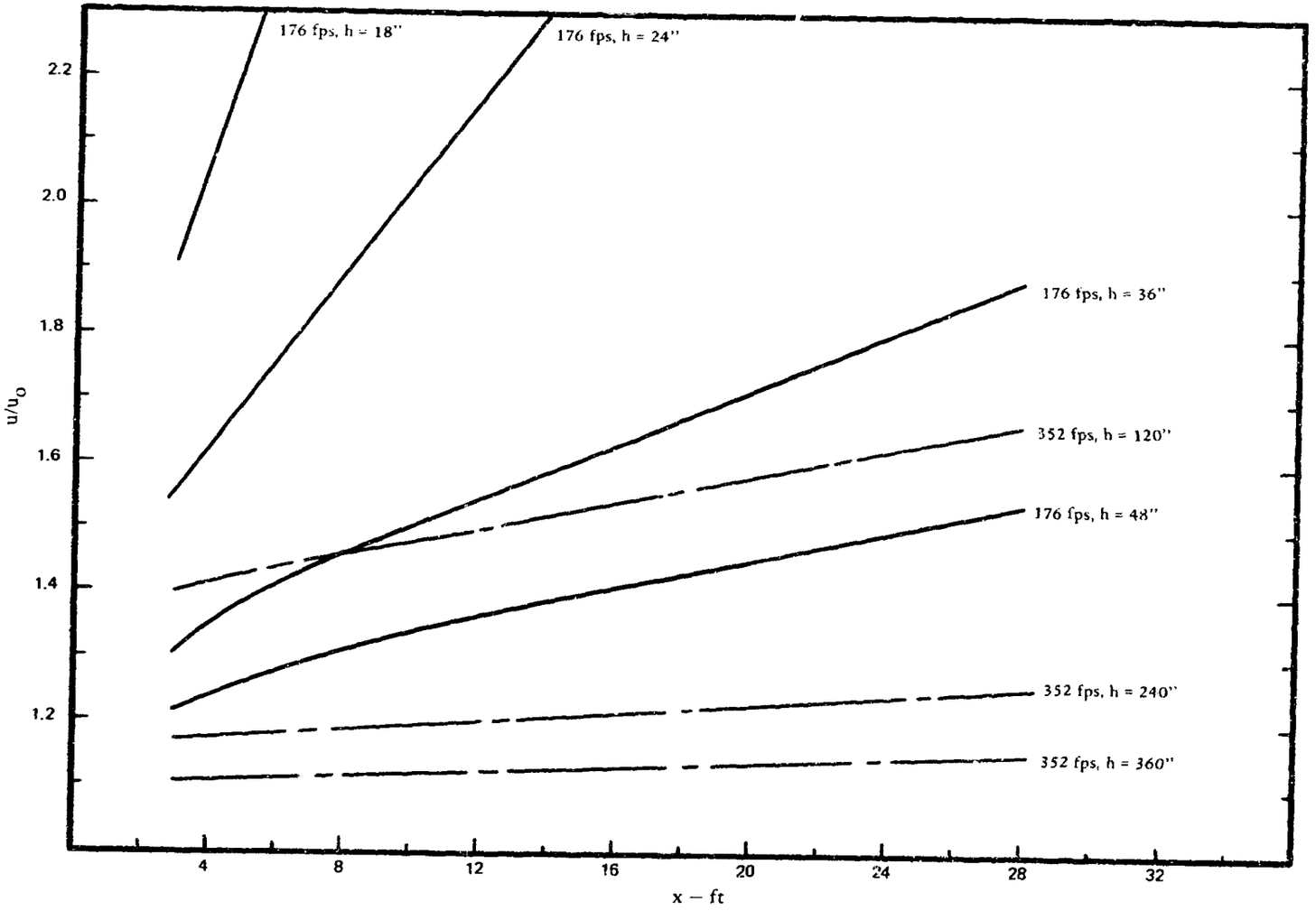

Figure 26. Calculated Relative Increase in Flow Velocity in Potential Core with Distance Along Particle Bed for Fixed Area Test Section with Initial Velocity and Tunnel Height as Parameters.

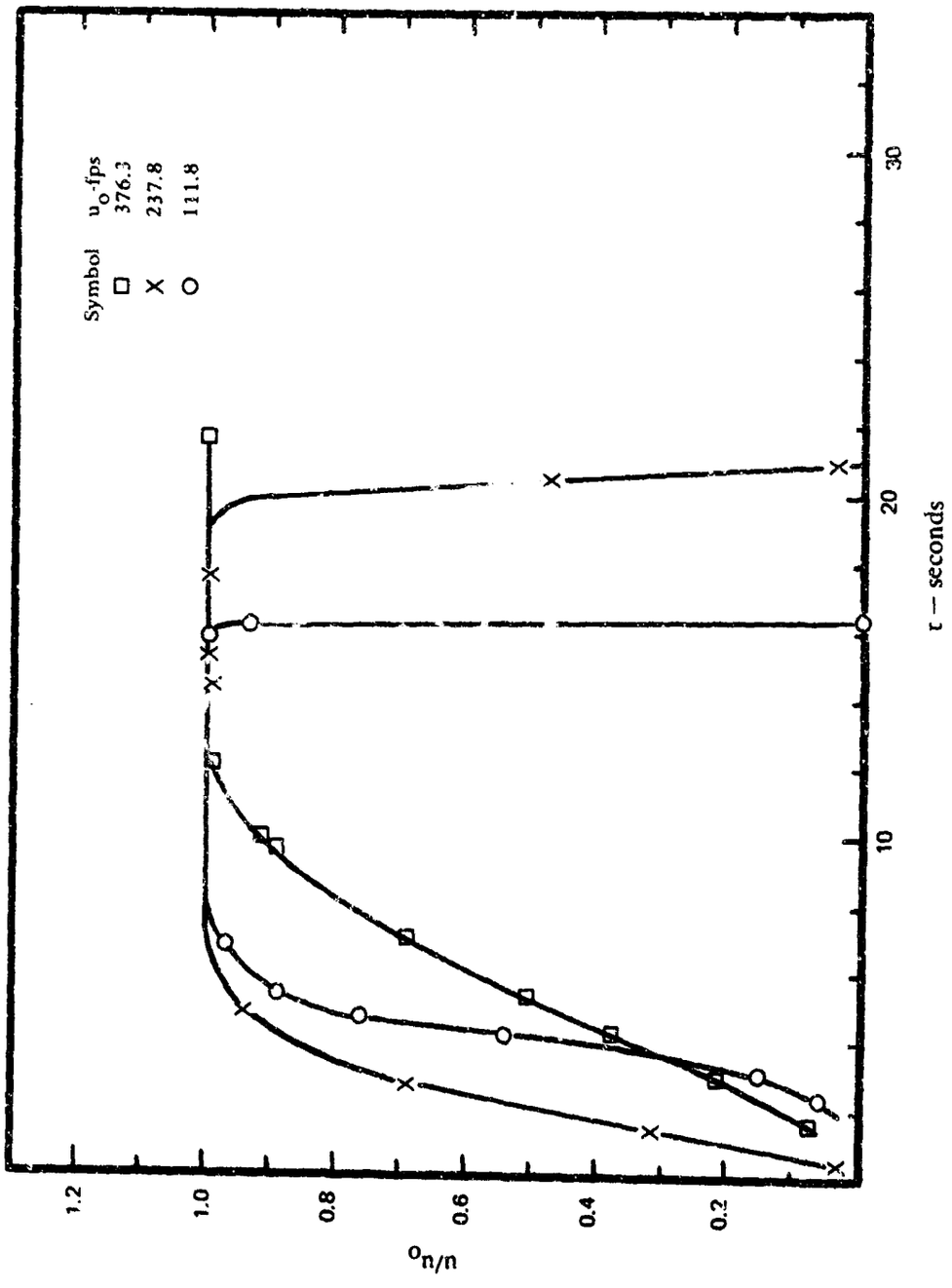

Figure 27. Measured Tunnel Flow Characteristics: Free Stream Velocity vs. Time.